MIDGArD: Modular Interpretable Diffusion over Graphs for Articulated Designs

Quentin Leboutet **Nina Wiedemann** **Zhipeng Cai** **Michael Paulitsch** **Kai Yuan**

Intel Labs – XRL – eXtended Reality Laboratory
{firstname.lastname}@intel.com

Abstract

Providing functionality through articulation and interaction with objects is a key objective in 3D generation. We introduce MIDGArD (Modular Interpretable Diffusion over Graphs for Articulated Designs), a novel diffusion-based framework for articulated 3D asset generation. MIDGArD improves over foundational work in the field by enhancing quality, consistency, and controllability in the generation process. This is achieved through MIDGArD's modular approach that separates the problem into two primary components: *structure generation* and *shape generation*. The structure generation module of MIDGArD aims at producing coherent articulation features from noisy or incomplete inputs. It acts on the object's structural and kinematic attributes, represented as features of a graph that are being progressively denoised to issue coherent and interpretable articulation solutions. This denoised graph then serves as an advanced conditioning mechanism for the shape generation module, a 3D generative model that populates each link of the articulated structure with consistent 3D meshes. Experiments show the superiority of MIDGArD on the quality, consistency, and interpretability of the generated assets. Importantly, the generated models are fully simulatable, i.e., can be seamlessly integrated into standard physics engines such as MuJoCo, broadening MIDGArD's applicability to fields such as digital content creation, meta realities, and robotics.

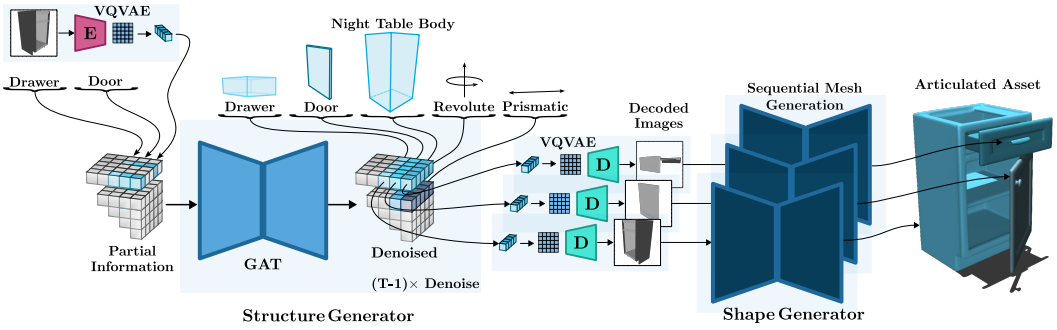

Figure 1: The MIDGArD generative pipeline.

1 Introduction

Despite their significance for applications in meta realities and embodied AI, the creation of 3D models of articulated objects remains a manual endeavor, and existing datasets [92, 97, 65, 102, 47, 63, 15] are often limited in both scope and scale. Human designers utilize strong prior knowledge of object geometry and kinematic structures, a capability that automated systems have yet to fully replicate.

38th Conference on Neural Information Processing Systems (NeurIPS 2024).

https://doi.org/10.52202/079017-0050

While extensive research has been conducted on generative models for static 3D objects [78, 74, 50, 48, 35, 8, 39, 54, 2, 95, 103, 24, 68, 9, 88, 75, 93, 6, 85, 98, 77, 52] and scenes [38, 31, 17, 71, 84, 14, 72, 53, 7, 12, 107], integrating 3D part geometry with kinematic structures has received far less attention. Generating articulated objects that are both geometrically detailed and kinematically accurate presents unique challenges due to the complexity of modeling part interactions and motions. Recent research efforts, such as Neural 3D Articulation Prior (NAP) [37] or Controllable Articulation GEneration (CAGE) [46], started addressing this gap, pioneering direct end-to-end generation of complete articulated assets using a denoising diffusion process acting on articulation graphs. However, generating consistent objects with high-fidelity shapes remains a challenge. Identified shortcomings of NAP [37] include 1) unnatural motion caused by unconstrained screw-like joint parametrization, 2) limited controllability, 3) limited interpretability and 4) the generation of inconsistent or unidentifiable shapes. Additionally, both NAP and related approaches lack *part*-level control due to the opaque encoding as a latent within the graph, highlighting the need for enhanced interpretability.

In this work, we introduce MIDGArD, a novel framework designed to generate interpretable and simulatable 3D articulated assets in a controllable manner. MIDGArD addresses the limitations of previous methods by offering: 1) improved consistency in joint motion, 2) enhanced controllability of the generation process, 3) increased interpretability and 4) better overall asset quality. Furthermore, the 3D assets generated by MIDGArD are fully simulatable and can be seamlessly integrated into virtual environments or physics engines such as MuJoCo [86], significantly enhancing its utility for digital content creation and robotics. MIDGArD employs a modular and sequential approach based on two diffusion models: the *structure generator* and the *shape generator* (see Figure 1). The *structure generator* denoises an articulation graph, unconditionally or from incomplete heterogenous inputs. This articulation graph acts as an abstract, yet interpretable object representation, encoding the structural and semantic information of every link, as well as kinematic attributes.

MIDGArD overcomes the identified limitations of prior works by 1) leveraging categorical embeddings for improving consistency across the articulation graph; 2) representing nodes (i.e. unique object parts) via latent image codes rather than direct mesh encoding; 3) diffusing on the Plücker manifold, thereby eliminating the need for discretizing the generated motion parameters, and 4) accounting for the orientation of the parts for more consistent generations. As additional benefit, these modifications yields an image representation, and asset-level, body-level, and joint-level categorical data, that are *human interpretable*. Since the generation process is sequential, these quantities can be adjusted by the user before generating proceeding with the part geometry generation. Crucially, this interpretable structure enables the use of a multi-modal 3D generation model as the *shape generator*. The shape generator, here represented by SDFusion [8], is queried multiple times to produce high-quality geometries for each part of the object (see Figure 1). To enhance consistency, we propose a constrained generation approach that enforces the part geometry to fit a given bounding box, here provided by the structure generator.

We demonstrate MIDGArD's capabilities by showcasing improved structural quality, consistency, and part-level control compared to NAP. Furthermore, we show qualitative results of MIDGArD generating diverse articulated objects dependent on the partial graph input and shape conditioning. To further improve the consistency and quality of the generated shapes, we propose a to create oriented bounding boxes that have a tighter fit to the ground truth while being properly aligned. The reduces the overlapping volume by 17% on average. Our contributions can be summarized as:

1. **MIDGArD:** A novel diffusion-based framework for generating high-quality, articulated, and simulatable 3D assets with improved consistency between structure and shape.
2. **Enhanced Interpretability, and Controllability:** Providing human-interpretable intermediate outputs and allowing user adjustments at multiple levels of the generation process.
3. **Enhanced Quality and Scalability:** Relying on state-of-the-art 3D foundation models for shape generation.
4. **Improved part alignment:** Introducing a bounding-box constrained shape generation approach that improves alignment of kinematic links by 17% on average.
5. **Simulatable Assets:** Offering a pipeline to create fully simulatable assets compatible with physics engines such as MuJoCo.

Code and models are available at `https://quentin-leboutet.github.io/MIDGArD`.

2 Related Works

Structural Characterization and State Estimation of Articulated Objects Designing articulated objects involves understanding both their geometry and kinematic properties. Traditional methods often require extensive manual labor or rely on limited datasets, hindering scalability and applicability [45]. Early work on morphable templates, such as SMPL for human bodies [55] and SMAL for quadruped animals [114], demonstrated the potential of matching existing articulation structures (i.e., skeletons) to a wide variety of inputs such as static meshes or monocular videos, thereby substantially simplifying the rigging process. However, while effective within specific categories, these templates lack the flexibility to generalize to arbitrary articulated mechanisms. To address these limitations, recent approaches have enhanced templates by incorporating implicit representations to model geometric deformations and appearances [40]. Robust neural rigging methods [61, 70] leverage template priors while remaining flexible enough to handle mesh elements that deviate from the template, such as clothing or hair. On the other hand, template-free methods [100, 101] rely solely on input mesh geometry but are still primarily limited to humanoid characters due to the scarcity of comprehensive datasets. Emerging approaches [27] aim to rig arbitrary static assets, potentially paving the way for a unified, template-free rigging pipeline. Our research aligns with this direction by learning articulation priors for arbitrary objects without depending on predefined templates.

Significant strides has also been made in estimating articulation joint states and parameters from sensory observations. Early contributions such as [83] demonstrated that it is possible to learn compact kinematic models of entire articulated objects solely based on pose observations. Probabilistic models have enabled robots to learn their own kinematic structures through self-observation and motor babbling [10, 81, 82]. Gaussian processes have been employed to model part connectivity and link articulation in objects [87]. Interactive perception techniques further enhance this learning process by allowing robots to interact with objects to obtain their kinematic model [69, 33, 64, 18, 66, 3, 22, 44, 25]. Deep learning techniques were also used to train dedicated architectures to directly predict articulation models from sensory inputs [23, 104, 1, 41, 49, 94, 106, 34, 29, 28, 51, 102, 13, 99, 105, 43, 20, 109]. Interactive systems [67, 13] learn to predict potential motions of articulated objects, aiding downstream motion planning and interaction, while reinforcement learning based approaches [96] train policies to explore diverse interaction trajectories, contributing to actionable visual representations. Our method diverges from traditional approaches by not relying on explicit estimation pipelines; instead, we learn articulation priors implicitly within our model.

Articulated Object Generation Generating articulated objects involves synthesizing models that accurately represent both geometric details and kinematic behaviors. Methods such as Self-Supervised Category-Level Articulated Object Pose Estimation [51] and PD (Pose-aware Part Decomposition) [34] address the generation of joint parameters and part poses, respectively, contributing significantly to the field. Few generative frameworks address both aspects concurrently. Notable among them is NAP [37], which generates complete articulated assets—including meshes—using graph attention networks. CAGE [46], enhances controllability and interpretability, albeit with limitations in mesh generation. More recently, [62] proposed a framework capable of reconstructing articulated assets from image inputs by using a 3D shape completion model to generate the different parts and a large language model (LLM) to predict the joint parameters. Progress was also made in physics-aware shape generation; for instance, [58] introduces an improved loss mechanism to account for internal collisions within generated articulated assets. In this work, we build up on NAP and CAGE and design an approach to enhance the controllability of the generative process, and leverage a multi-modal 3D generative model for improving the quality of the shape geometry.

3D Shape Generation and Completion Recent progress in diffusion models and 2D-guided generation techniques have revolutionized 3D shape generation and completion. Two main types of generative pipelines are currently being explored. The first one leverages 2D diffusion models to optimize NeRFs [73, 42, 57], enabling high-quality 3D generation without the need for direct 3D supervision. The second employs Latent Diffusion Models (LDMs) for different 3D representations, including point clouds [59, 113, 112, 60, 88], voxels [111], SDFs[8, 76, 111, 48], shape2vecset[108, 110], and triplanes [16]. It should be emphasized that despite the predominant role of diffusion models, other methodologies such as autoregressive models [78], have demonstrated potential in producing high-fidelity 3D shapes from minimal inputs. Conditional diffusion models enable multi-modal inputs. SDFusion [8], for instance, can generate 3D objects from text descriptions, images, or partial 3D shapes. Building upon these capabilities, we have adapted SDFusion as the shape generator within our framework. However, due to MIDGArD's modular design, the shape generator can be updated to incorporate the latest advancements in static 3D generation.

https://doi.org/10.52202/079017-0050

3 Synthesis of 3D Articulated Mechanisms

3.1 Method Overview

Both components of MIDGArD, namely the structure and the shape generator, leverage a denoising diffusion model [79, 80, 21]. Diffusion models operate by progressively degrading training data through the systematic application of Gaussian noise, a method known as the forward process. Subsequently, these models are trained to restore the original data by methodically removing this noise in what is known as the reverse process. Please refer to Appendix A and [21], [79] for details. As shown in Figure 1, the full MIDGArD pipeline can be separated into the *Structure Generator* and the *Shape Generator*. The Structure Generator (subsection 3.2) takes graph-based representation of an articulated asset – which may be incomplete or affected by noise – and resolves this representation through diffusion. The denoised graph features, decoded into suitable – human interpretable – text prompts, images and bounding box information are then fed into the Shape Generator (subsection 3.3), another diffusion-based model yielding the final articulated 3D object.

3.2 Structure Generator

Articulated Asset Representation and Parametrization Building upon [37], we encode the structural and kinematic attributes of every articulated asset into the node and edge features of a complete graph referred to as $\boldsymbol{G}_N$. Our structure generation module leverages a Graph ATtention (GAT) [90, 4, 32] denoising network to generate coherent and interpretable articulation features from noisy or incomplete inputs (see Figure 1). To improve the quality, controllability, and interpretability compared to [37], we modify the asset parametrization. Drawing on insights from [46], we incorporate a set of categorical variables to the nodes and edges features to enhance asset consistency, interpretability and provide a more intuitive control interface over the generation process. Each asset is represented as a complete graph $\boldsymbol{G}_N = \{\boldsymbol{x}, \boldsymbol{e}\}_N$ that embodies the object's links and joints in its N nodes, and in its $N(N-1)/2$ edges respectively. Rather than directly denoising and then decoding a low-dimensional shape latent $\boldsymbol{f}_i \in \mathbb{R}^{D_F}$ for each link i into a 3D mesh [37, 36], we propose a two-step approach that operates on a more manageable image latent $\boldsymbol{g}_i \in \mathbb{R}^{D_G}$ of the link. This image latent is derived by training a Vector-Quantized Variational Auto Encoder (VQVAE) [89] on various views of every rigid body in the dataset. In our method, the structure generator denoises a latent representation of an image for each individual component of the articulated asset. This denoised image, along with the categorical information extracted from the graph, facilitates the creation of human-interpretable priors for each link, namely a text description and a front view image. These prompts can then be utilized to condition a 3D shape generation model yielding consistent meshes. Additionally, the graph itself encodes highly relevant structural features that act as supplementary conditioning signals, further guiding the shape generation model.

Each node $\boldsymbol{x}_i$ represents a link of the articulated asset and $\forall i, j \in [0, N-1]$ the edge $\boldsymbol{e}_{ij}$ establishes a connection between node $\boldsymbol{x}_i$ and node $\boldsymbol{x}_j$. The node feature vector $\boldsymbol{x}_i$ is comprised of multiple components, specifically, $\boldsymbol{x}_i = [\boldsymbol{o}_i, \boldsymbol{a}_i, \boldsymbol{b}_i, \boldsymbol{d}_i, \boldsymbol{r}_i, \boldsymbol{t}_i, \boldsymbol{g}_i] \in \mathbb{R}^{D_V}$, and the edge feature vector $\boldsymbol{e}_{ij}$ is formulated as $\boldsymbol{e}_{ij} = \left[\boldsymbol{c}_{ij}, \boldsymbol{j}_{ij}, \boldsymbol{p}_{ij}, \boldsymbol{l}_{ij}\right] \in \mathbb{R}^{D_E}$, where D_V and D_E refer to the node and edge feature dimensions. To ensure a consistent graph size across various objects, N is set to the maximum count of parts anticipated, using $\boldsymbol{o}_i \in [0, 1]$ as a binary indicator to denote part existence. Similarly, the edges denote symbolic existence and chirality through the indicator variable $\boldsymbol{c}_{ij} \in [0, 1]^3$. Joint types are represented through $\boldsymbol{j}_{ij} \in [0, 1]^{D_J}$, a one-hot encoding that in our design has a dimensionality of three to signify the types – prismatic, revolute, or screw. Similarly, $\boldsymbol{a}_i \in [0, 1]^{D_A}$ and $\boldsymbol{b}_i \in [0, 1]^{D_B}$ denote the one-hot encoding vectors of asset (resp. body) categories. Similar to [37], we use Plücker coordinates as joint parametrization as this provides a compact representation for joint types, such as revolute, prismatic, and screw joints. The Plücker joint parametrization, articulated as $\boldsymbol{p}_{ij} \in \mathbb{R}^6$, provides a harmonious portrayal of the different joint types under consideration, and joint limits are entailed by $\boldsymbol{l}_{ij} \in \mathbb{R}^{D_L}$. Ultimately, the vectors $\boldsymbol{d}_i \in \mathbb{R}^3$, $\boldsymbol{r}_i \in \mathbb{R}^3$ and $\boldsymbol{t}_i \in \mathbb{R}^3$ depict the bounding box dimensions, orientation and position of each part. Note that $\boldsymbol{r}_i$ and $\boldsymbol{t}_i$ are defined for every part relative to its parent reference frame.

Unlike previous approaches [37, 46], we do not assume that the parts of the dataset are provided in a canonical orientation. Assuming that objects are in canonical orientation and not explicitly considering the orientation leads to degrading performance due to misaligned orientations of the dataset (see Figure 5, as well as Appendix B-Figure 10 and Appendix B-Figure 11). Instead, we

estimate this orientation for each body in the dataset by computing the corresponding Oriented Bounding Box (OBB), which is then used to position the body in a canonical pose. The process (see Appendix B) begins by generating a convex hull from the mesh. This step simplifies the complex geometry into a more manageable form, reducing dependency on the internal structure of the object. Next, we voxelize the convex hull to collect volumetric samples. We then execute a Principal Component Analysis (PCA) to determine the primary axes of the mesh providing an initial approximation of the object's orientation. Following the PCA, we perform gradient descent on the attitude quaternion of the OBB, using the PCA-based initial estimate as a starting point. The objective of this optimization is to minimize the volume of the OBB. This approach allows for a more flexible and accurate alignment of dataset bodies into canonical poses, thereby enhancing the overall quality and consistency of the articulated objects generated by our framework (see Figure 5, Table 3).

Denoising Diffusion on the Plücker Manifold To maintain the interpretability of the denoised quantity as a Plücker vector $\boldsymbol{p}_{ij} = [\boldsymbol{u}_{ij}, \boldsymbol{v}_{ij}]$, our approach introduces a novel parametrization allowing the diffusion process to be directly executed on the Plücker manifold $\mathcal{P}$. In contrast, the approach proposed in [37], denoises within $\mathbb{R}^6$, thereby requiring a projection operation $p : \mathbb{R}^6 \to \mathcal{P}$ at every denoising step. We propose an alternative formulation $\boldsymbol{k}_{ij} = [\boldsymbol{m}_{ij}, \boldsymbol{n}_{ij}] \in \mathbb{R}^5$ of the joint parameters where $\boldsymbol{m}_{ij} = [\theta_{ij}, \varphi_{ij}] \in \mathbb{R}^2$ represent the spherical parametrization of the Plücker axis $\boldsymbol{u}_{ij}$. This formulation yields $\boldsymbol{u}_{ij} = [\sin(\theta_{ij})\cos(\varphi_{ij}), \sin(\theta_{ij})\sin(\varphi_{ij}), \cos(\theta_{ij})] \in \mathbb{R}^3$ with $\|\boldsymbol{u}_{ij}\| = 1$. The vector $\boldsymbol{n}_{ij} \in \mathbb{R}^3$ is then defined such that $\boldsymbol{v}_{ij} = \boldsymbol{n}_{ij} \times \boldsymbol{u}_{ij}$. This alternative parametrization guarantees the normalization of $\boldsymbol{u}_{ij}$ and enforces by construction the orthogonality between $\boldsymbol{u}_{ij}$ and $\boldsymbol{v}_{ij}$, which are key features of the Plücker manifold [30]. Consequently, our approach inherently satisfies the manifold's constraints, thereby streamlining the computational workflow by eliminating the necessity for iterative projections.

3.3 Shape Generator

The shape generator of MIDGArD aims to create the mesh for each component of an articulated object using the denoised object graph, which contains both semantic (object category) and visual (image latents) data. We leverage a multi-modal 3D generative model that is trained independently from the structure generator. Our modular setup is designed to accommodate any generative model, allowing for seamless integration of the latest advances in 3D generation. In this work, the SDFusion model [8] is used, conditioned on image, text as well as graph features input, and enhanced with a novel approach for bounding-box-constrained generation. The training pipeline is shown in Figure 2.

Multimodal Guidance for Consistent Shape Generation The core of SDFusion is a latent diffusion model, see [8] for details. Object meshes are transformed into truncated signed distance functions (TSDFs) and encoded using a pretrained and frozen 3D VQ-VAE [89] model. The diffused latent representations, along with image and text condition signals, are denoised through a 3D U-Net model. The resulting output latent is then decoded into a TSDF and converted back into a mesh using a marching cube algorithm [56]. It is worth emphasizing that we train and apply the diffusion model on the individual *parts* of each objects, querying the model multiple times at inference time to generate a full articulated object (see Figure 1). The model is trained on the PartNet Mobility dataset [97] with the same train-test split as the structure generator. We modified SDFusion's conditioning [8] to align it with the output of the structure generator. The model is conditioned through cross-attention on the following modalities, either independently or in combination.

- Single view image: A pretrained ResNet-18 model [19] encodes images. During training, the model uses renderings of the part mesh from a frontal view. At inference, the model decodes the image from the node features of the articulation graph.
- Text: We employ BERT [11] for text encoding (similar to [84, 8]). The text is constructed using the object category and asset type from the PartNet dataset in the format "A `<asset type>` as part of a `<object category>`"; for instance, "*A lid as part of a trash can*".
- Graph: The output from the structure generator is encoded and concatenated with image- and text embeddings to provide information about the part's role within the object, such as its expected size and its relation to other parts, i.e. joint types.

This multi-modal conditioning approach ensures the generation of consistent, high-quality parts that can be seamlessly integrated to form complete articulated objects, enhancing the overall performance and applicability of our framework.

https://doi.org/10.52202/079017-0050

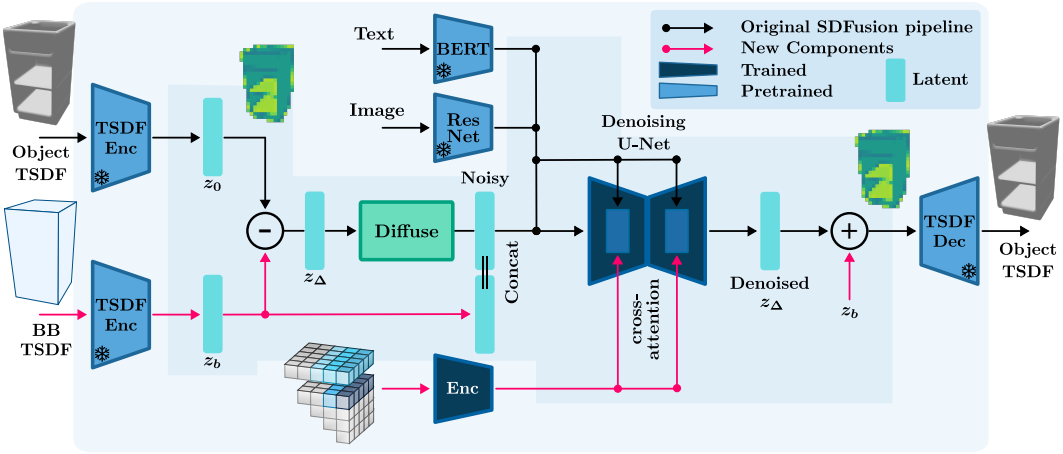

Figure 2: Architecture of the Shape Generator.

Enforcing Bounding Constraints Generating object parts independently offers increased flexibility and quality but introduces challenges related to the size and orientation of the generated parts. Intuitively, the shape generator must ensure that parts conform to $\boldsymbol{r}_i$ and $\boldsymbol{d}_i$ in the articulation graph. To achieve the correct *orientation*, we generate links in a canonical pose and subsequently apply a post-processing rotation based on $\boldsymbol{r}_i$, the 3D orientation vector derived during structure generation. To train the model accordingly, by estimating and adjusting the pose of parts to a canonical orientation, as detailed in Appendix B.

To ensure that generated parts match the *sizes* specified within the graph node features, we introduce a bounding-box constraint to the generative model (see Figure 2). Instead of generating the object directly, the diffusion model is trained on the *difference* relative to a predefined bounding box. To enable this schema for *latent* diffusion, we calculate the difference as $z_\Delta = z_o - z_b$, where z_o is the VQ-VAE-encoded latent of the object, and z_b is the encoding of a simplified bounding-box TSDF (values inside the box set to -0.01, and values outside set to 0.01). During inference, we provide the denoiser with the bounding box information by concatenating z_b to the noisy version of z_Δ. Other conditioning inputs, such as images, text, and graph features encodings, are incorporated through cross-attention mechanisms. The object's TSDF is then computed by decoding $z_\Delta + z_b$ using the 3D VQ-VAE. This method effectively guides the model to produce objects that are closely matching the target bounding boxes even after a few training steps.

4 Experiments, Results and Discussion

4.1 Experiment Setup

Dataset All experiments were conducted using the PartNet Mobility dataset [97], which contains a diverse set of articulated 3D objects with detailed geometric and kinematic annotations. Each mesh in the dataset underwent a two-step preprocessing routine. First, we enforced the manifold property as described in [26]. Second, we performed orientation estimation to establish a canonical pose for each object and accurately compute the corresponding bounding boxes (see Appendix B for details).

Evaluation Metrics We adopt the evaluation framework from NAP [37], which introduces the Instantiation Distance (ID) metric for comparing two articulated objects. ID measures the average Chamfer distance over sampled joint states, accounting for both geometric and kinematic differences. It is defined as:

$$ID(O_1, O_2) \approx \frac{1}{M} \sum_{q_1 \in Q_1} \left[\min_{q_2 \in Q_2} \left(\tilde{d}(O_1, q_1, O_2, q_2) \right) \right] + \frac{1}{M} \sum_{q_2 \in Q_2} \left[\min_{q_1 \in Q_1} \left(\tilde{d}(O_1, q_1, O_2, q_2) \right) \right], \quad (1)$$

where Q is a set of M uniformly sampled joint poses and $\tilde{d}$ is the minimum Chamfer distance over all possible canonicalizations of the mesh. We use ID in conjunction with standard metrics for unconditional generation, namely minimum matching distance (MMD), coverage (COV) and 1-nearest-neighbor accuracy (1-NNA).

Implementation Details We trained the structure generator and the image VQ-VAE on an NVIDIA RTX 3090 GPU, while the shape generator was trained on an NVIDIA RTX 6000 GPU. Evaluation took place on a single NVIDIA RTX 3090 GPU. The image VQ-VAE, which encodes latent representations of objects in the shape generator, was trained on 256×256-pixel front renderings of the the PartNet Mobility object meshes. The denoising model used in the structure generator contains six graph attention blocks, with a latent embedding size of 512 and 32 attention heads. We set the maximum number of nodes in the graph to $N = 8$. Our training parameters closely follow those in NAP, with the key difference being the use of an implicit denoising diffusion pipeline [80] over 100 time steps, as opposed to a DDPM with 1,000 time steps. This modification significantly accelerates inference speed. Our shape generator is adapted from SDFusion [8] and trained on the PartNet Mobility dataset. We used the same hyperparameters as the multimodal model in SDFusion and utilized their pre-trained VQ-VAE checkpoint. We excluded 10 categories from training due to their objects containing numerous equally-shaped parts (e.g., keyboards with over 30 keys).

4.2 Results and Discussion

Unconditional Articulated Asset Generation To the best of our knowledge, NAP is the only approach for generating articulated 3D objects without prior knowledge about their geometric structure. We first evaluate MIDGArD in an unconditional generation setting, comparing its performance to NAP. For a fair comparison, we retrained NAP on our preprocessed version of the PartNet Mobility dataset. The results are presented in Table 1. MIDGArD outperforms NAP in terms of MMD and COV metrics, indicating better diversity and coverage of the generated samples. Specifically, we observe a 6.4% improvement in MMD and a 3.7% improvement in COV. The 1-NNA metric is comparable between both methods. We also perform an ablation study on the effect of the Plücker manifold parameterization. As shown in Table 1 using the Plücker manifold improves the MMD and COV metrics, suggesting enhanced consistency and diversity in the generated assets.

Table 1: Comparison to NAP in an unconditional generation setting.

Generative Paradigm/Method	Unconditional ID		
	MMD ↓	COV ↑	1-NNA ↓
NAP	0.0282	0.4675	**0.5831**
Ours (Plücker manifold)	**0.0264**	**0.4857**	**0.5831**
Ours (No Plücker manifold)	0.0270	0.4779	0.6221

To further evaluate the physical plausibility of the generated assets, we analyze the distribution of joint types in the training data and compare it with those in samples generated by NAP and MIDGArD. We sampled 400 objects generated by each method and counted each joint type only once per object to minimize the impact of objects with multiple joints of the same type.

Table 2: Distribution of joint categories in real data vs generated data from NAP and our approach.

	Screw	Revolute	Prismatic
Training data	6%	62%	32%
NAP-generated	95%	1%	4%
MIDGArD-generated	**2%**	**62%**	**36%**

The results in Table 2 show that NAP predominantly produces screw joints, which are rare in the training data. In contrast, MIDGArD generates objects with a joint type distribution closely matching that of the training data, thereby enhancing the plausibility of the generated assets. We computed the Chi-Square statistic to quantify the deviation from the expected joint type distribution. NAP's generated data yielded a high χ^2 value of 5618, indicating a significant difference from the training data distribution. In contrast, MIDGArD's generated data resulted in a low χ^2 value of 12.7, demonstrating close alignment with the expected distribution.

Figure 3.B provides a side-by-side qualitative comparison between MIDGArD and NAP. MIDGArD generates objects with higher geometric quality and more realistic motion compared to NAP. For instance, the fan generated by MIDGArD exhibits detailed geometry, and the laptop displays realistic opening motion, whereas NAP's outputs often show unnatural joint motions and inconsistent shapes.

https://doi.org/10.52202/079017-0050

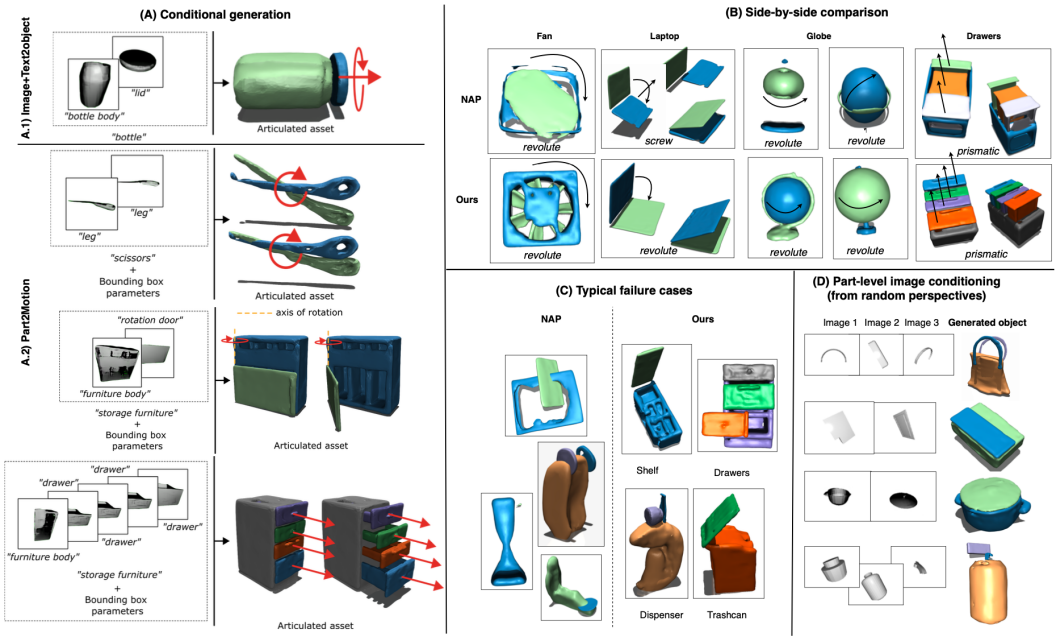

Figure 3: A) *PartToMotion* constrained structural generation. B) Side-by-side comparison between our approach and NAP. C) Typical failure cases. D) Part-level image conditioning.

Additionally, as shown in Figure 3.C, the absence of categorical information in NAP leads to the generation of objects composed of mismatched parts that do not cohesively fit together. In our approach, while there may be occasional issues with geometry or kinematics, the object parts remain semantically consistent, preserving the integrity of the overall structure. Finally, as illustrated in Figure 3.D, our conditional part-generation proves to be robust to images from different viewpoints, yielding enhanced flexibility and generalization capability of our method.

Conditional Generation and Controllability One of the key advantages of MIDGArD over existing approaches is its enhanced controllability, enabling users to guide the generation process using human-understandable graph attributes such as articulated asset types and body types. We showcase this capability in a "`(Image+Text)-To-Object`" setup (see Figure 3.A1), and a "`Part-To-Motion`" setup (see Figure 3.A2), where the model is provided with part features only (i.e., no joint data) and outputs consistent articulated assets. Notably, MIDGArD can also be controlled using only asset-level data; for instance, users can query for specific categories such as "`storage furniture`" or "`fan`" without needing to provide detailed information for each node (see Appendix C for additional qualitative results). Furthermore, the modular structure of our generation pipeline enables fine-grained, part-level control. Users can specify the desired appearance or attributes of individual parts by adjusting the human-interpretable articulation solutions synthesized by the structure generator accordingly. The resulting images and text description will then be used as conditioning signals for the shape generation module. As illustrated in Figure 4, varying the image inputs while keeping other attributes fixed results in generated parts that adapt accordingly, demonstrating the flexibility and responsiveness of our approach. This level of control allows for precise customization of generated assets, facilitating applications that require specific design features or aesthetic qualities (see Appendix D for additional qualitative results).

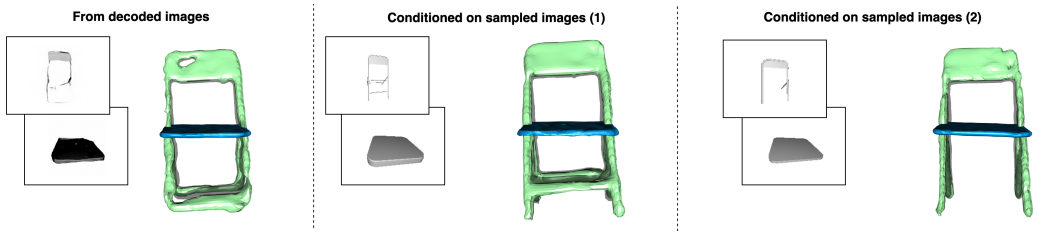

Figure 4: Image guidance of the shape generation process

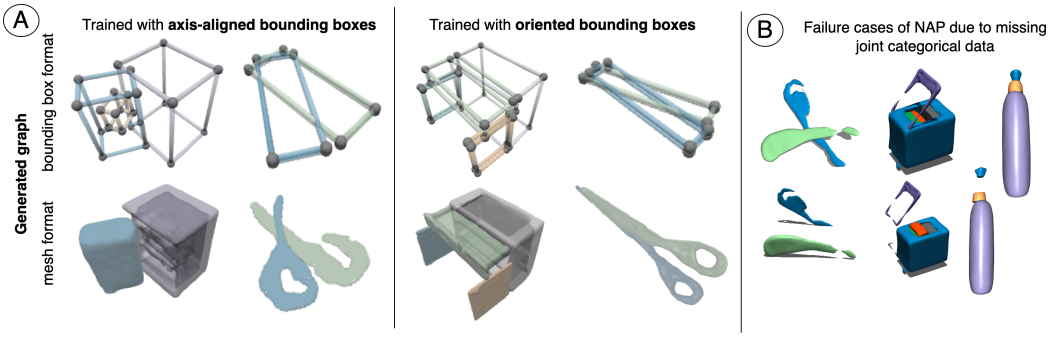

Figure 5: Failure cases due to due to axis-aligned bounding boxes and parameter discretization. A) The use of Axis Alligned Bounding Boxes tends to confuse the 3D generation model. B) The use of categorical joint variable in MIDGArD allows better joint motion resolution and helps filtering unrealistic solutions obtained with former pipelines.

Constrained Shape Generation We conducted an ablation study to evaluate the effectiveness of our bounding-box constrained shape generation approach introduced in section 3.3. The experiments were performed on *part*-samples from PartNet Mobility. We randomly sampled ten objects per category from the test data, including all their parts, resulting in 1044 samples across 32 categories. First, we measure whether the generated object fits within the bounding box. The model output Y^{gen} is a sampled TSDF of resolution 64, $Y^{gen} \in \mathbb{R}^{64\times64\times64}$, where negative values indicate the object's interior. We compare Y^{gen} with the TSDF of the bounding box Y^{bb} and compute the count of all cells outside of the bounding box (OBB_{count}) and their sum of SDF values (OBB_{sum}):

$$OBB_{count}(O_{bb}, O_{gen}) = \sum_{ijk} \mathbb{1}[Y^{bb}_{ijk} > 0 \wedge Y^{gen}_{ijk} < 0], \tag{2}$$

$$OBB_{sum}(O_{bb}, O_{gen}) = \sum_{ijk} Y^{gen}_{ijk} \cdot \mathbb{1}[Y^{bb}_{ijk} > 0 \wedge Y^{gen}_{ijk} < 0]. \tag{3}$$

Secondly, we evaluate the generation quality after transforming the TSDF into a mesh, computing the Chamfer distance (CD) between generated and real objects based on 5000 sampled points. Table 3 compares our *bb prior* approach to the original SDFusion model trained on PartNet Mobility. For encoding the part dimensions, we use an MLP with three hidden layers (size 16, 64 and 256 respectively). For a comparison to a GAT-encoding, see Appendix E. Our first modification of preprocessing the dataset to rectify objects into canonical pose, dubbed "original + bb MLP + oriented dataset", already improves the generation results significantly, leading to lower OBB_{count}, OBB_{sum} and CD. The *bb prior* method, however, consistently ensures accurate proportions and sizes for the generated links, diminishing erroneous volume. Additionally, *bb prior + bb MLP* method secures the best Chamfer Distance at 0.072. An alternative technique involves resizing generated objects to suit the bounding box dimensions. Such postprocessing of the model outputs reduces the average CD to 0.0061, close to matching that of the *bb prior* method. Nonetheless, such resizing may lead to significant distortions in object proportions, thereby underscoring the superiority of the *bb prior* method.

Analysis of Oriented Bounding Boxes As Table 3 shows, using oriented bounding boxes drastically improves the reconstruction performance. To quantify the change to the dataset, we measured the volume reduction of the bounding boxes after applying our PCA-based rectification approach. On average, the bounding box volume decreased by 17.4%, with one-third of the samples experiencing

Table 3: Ablation of bounding-box constrained shape generation. The original SDFusion pipeline, only enhanced with bounding-box conditioning, is compared to our approach. Training on a preprocessed dataset and post-processing the generated shapes afterwards already improves the performance significantly. The best results are achieved using our bounding-box SDF prior with post-processing.

	OBB_{count}	OBB_{sum}	CD (generated)	CD (scaled)
bb prior + bb MLP (Ours)	**1146**	**10.89**	**0.0072**	**0.0043**
original + bb MLP + oriented dataset	1490	37.15	0.0152	0.0061
original (SDFusion) + bb MLP	3795	183.5	0.0307	0.008

https://doi.org/10.52202/079017-0050

a volume decrease of more than 10% and 20% of the samples experiencing a volume decrease of more than 30%. Figure 5 illustrates failure cases where using axis-aligned bounding boxes leads to unrealistic part shapes, such as a thick cabinet door.

5 Conclusions

In this work, we introduced MIDGArD, a novel framework for generating 3D articulated objects. MIDGArD employs a modular approach, combining interpretable articulation graph generation with high-quality shape generation. By leveraging categorical parametrization, MIDGArD enhances the consistency and plausibility of articulated objects, producing high-quality meshes with accurate dimensions through a constrained shape generation mechanism. The human-interpretable representation of images and text within the articulation graph allows for part-level and multi-modal control over the generation process. The models produced by MIDGArD are fully simulatable, paving the way for applications in text-guided or image-guided content creation.

MIDGArD addresses several issues identified in Neural 3D Articulation Prior (NAP) by improving joint conditioning with categorical embeddings, enforcing physical constraints via bounding-box constrained generation, and providing part-level control using latent image codes. Our results demonstrate MIDGArD's superior performance in terms of structural quality, consistency, and interpretability compared to existing methods. The framework's ability to generate diverse articulated objects based on partial graph inputs and shape conditioning underscores its potential for broad applications in digital content creation and robotics.

Despite the advancements introduced by MIDGArD, there are several limitations and areas for future improvement: 1) We observe that the current metrics for articulated generation are still very limited and benchmarks as well as evaluation frameworks must be developed for this field. For instance, Instantiation Distance is still based on point clouds, which ignores cases of *small* parts of the object with unrealstic motion, such as a cart wheel moving up to a meter away from the cart. 2) Overcoming limitations of graph scalability posed by node number constraints remains an important challenge. 3) Furthermore, it would be interesting to investigate the use of mixed integer noise methods such as MiDi [91] in the articulation graph generation pipeline to process the continuous and discrete variables. 4) Enhanced conditioning of the structure generation process using natural language or image data represents a highly promising avenue for future research. Foundational efforts in this area, such as those by Cai et al. [5], have laid the groundwork for further exploration. 5) Integrating specialized templates, such as human body poses, could significantly enhance MIDGArD's modelling versatility. Lastly, 6) testing alternative 3D generation models and adapting MIDGArD to handle different geometric primitives could broaden its generalization capabilities.

References

[1] Ben Abbatematteo, Stefanie Tellex, and George Konidaris. Learning to generalize kinematic models to novel objects. In *Proceedings of the 3rd Conference on Robot Learning*, 2019.

[2] Mohammad Samiul Arshad and William J Beksi. List: Learning implicitly from spatial transformers for single-view 3d reconstruction. In *Proceedings of the IEEE/CVF International Conference on Computer Vision*, pages 9321–9330, 2023.

[3] Jeannette Bohg, Karol Hausman, Bharath Sankaran, Oliver Brock, Danica Kragic, Stefan Schaal, and Gaurav S Sukhatme. Interactive perception: Leveraging action in perception and perception in action. *IEEE Transactions on Robotics*, 33(6):1273–1291, 2017.

[4] Shaked Brody, Uri Alon, and Eran Yahav. How attentive are graph attention networks? *arXiv preprint arXiv:2105.14491*, 2021.

[5] Zhou Cai, Xiyuan Wang, and Muhan Zhang. Latent graph diffusion: A unified framework for generation and prediction on graphs. *arXiv preprint arXiv:2402.02518*, 2024.

[6] Rui Chen, Yongwei Chen, Ningxin Jiao, and Kui Jia. Fantasia3d: Disentangling geometry and appearance for high-quality text-to-3d content creation. *arXiv preprint arXiv:2303.13873*, 2023.

[7] Yamei Chen, Yan Di, Guangyao Zhai, Fabian Manhardt, Chenyangguang Zhang, Ruida Zhang, Federico Tombari, Nassir Navab, and Benjamin Busam. Secondpose: Se (3)-consistent dual-stream feature fusion for category-level pose estimation. *arXiv preprint arXiv:2311.11125*, 2023.

[8] Yen-Chi Cheng, Hsin-Ying Lee, Sergey Tulyakov, Alexander G Schwing, and Liang-Yan Gui. SDFusion: Multimodal 3d shape completion, reconstruction, and generation. In *Proceedings of the IEEE/CVF Conference on Computer Vision and Pattern Recognition*, pages 4456–4465, 2023.

[9] Ruihang Chu, Enze Xie, Shentong Mo, Zhenguo Li, Matthias Nießner, Chi-Wing Fu, and Jiaya Jia. Diffcomplete: Diffusion-based generative 3d shape completion. *Advances in Neural Information Processing Systems*, 36, 2024.

[10] Anthony Dearden and Yiannis Demiris. Learning forward models for robots. In *IJCAI*, volume 5, page 1440, 2005.

[11] Jacob Devlin, Ming-Wei Chang, Kenton Lee, and Kristina Toutanova. Bert: Pre-training of deep bidirectional transformers for language understanding. *arXiv preprint arXiv:1810.04805*, 2018.

[12] Yan Di, Chenyangguang Zhang, Chaowei Wang, Ruida Zhang, Guangyao Zhai, Yanyan Li, Bowen Fu, Xiangyang Ji, and Shan Gao. Shapemaker: Self-supervised joint shape canonicalization, segmentation, retrieval and deformation. *arXiv preprint arXiv:2311.11106*, 2023.

[13] Ben Eisner, Harry Zhang, and David Held. Flowbot3d: Learning 3d articulation flow to manipulate articulated objects. *arXiv preprint arXiv:2205.04382*, 2022.

[14] Chuan Fang, Xiaotao Hu, Kunming Luo, and Ping Tan. Ctrl-room: Controllable text-to-3d room meshes generation with layout constraints. *arXiv preprint arXiv:2310.03602*, 2023.

[15] Haoran Geng, Helin Xu, Chengyang Zhao, Chao Xu, Li Yi, Siyuan Huang, and He Wang. Gapartnet: Cross-category domain-generalizable object perception and manipulation via generalizable and actionable parts. In *Proceedings of the IEEE/CVF Conference on Computer Vision and Pattern Recognition*, pages 7081–7091, 2023.

[16] Anchit Gupta, Wenhan Xiong, Yixin Nie, Ian Jones, and Barlas Oğuz. 3dgen: Triplane latent diffusion for textured mesh generation. *arXiv preprint arXiv:2303.05371*, 2023.

 https://doi.org/10.52202/079017-0050

[17] Kamal Gupta, Justin Lazarow, Alessandro Achille, Larry S Davis, Vijay Mahadevan, and Abhinav Shrivastava. Layouttransformer: Layout generation and completion with self-attention. In *Proceedings of the IEEE/CVF International Conference on Computer Vision*, pages 1004–1014, 2021.

[18] Karol Hausman, Scott Niekum, Sarah Osentoski, and Gaurav S Sukhatme. Active articulation model estimation through interactive perception. In *2015 IEEE International Conference on Robotics and Automation (ICRA)*, pages 3305–3312. IEEE, 2015.

[19] Kaiming He, Xiangyu Zhang, Shaoqing Ren, and Jian Sun. Deep residual learning for image recognition. In *Proceedings of the IEEE conference on computer vision and pattern recognition*, pages 770–778, 2016.

[20] Nick Heppert, Muhammad Zubair Irshad, Sergey Zakharov, Katherine Liu, Rares Andrei Ambrus, Jeannette Bohg, Abhinav Valada, and Thomas Kollar. Carto: Category and joint agnostic reconstruction of articulated objects. In *Proceedings of the IEEE/CVF Conference on Computer Vision and Pattern Recognition*, pages 21201–21210, 2023.

[21] Jonathan Ho, Ajay Jain, and Pieter Abbeel. Denoising diffusion probabilistic models. *Advances in neural information processing systems*, 33:6840–6851, 2020.

[22] Cheng-Chun Hsu, Zhenyu Jiang, and Yuke Zhu. Ditto in the house: Building articulation models of indoor scenes through interactive perception. *arXiv preprint arXiv:2302.01295*, 2023.

[23] Ruizhen Hu, Wenchao Li, Oliver Van Kaick, Ariel Shamir, Hao Zhang, and Hui Huang. Learning to predict part mobility from a single static snapshot. *ACM Transactions on Graphics (TOG)*, 36(6):1–13, 2017.

[24] Yubin Hu, Sheng Ye, Wang Zhao, Matthieu Lin, Yuze He, Yu-Hui Wen, Ying He, and Yong-Jin Liu. Oˆ 2-recon: Completing 3d reconstruction of occluded objects in the scene with a pre-trained 2d diffusion model. *arXiv preprint arXiv:2308.09591*, 2023.

[25] Jiahui Huang, He Wang, Tolga Birdal, Minhyuk Sung, Federica Arrigoni, Shi-Min Hu, and Leonidas J Guibas. Multibodysync: Multi-body segmentation and motion estimation via 3d scan synchronization. In *Proceedings of the IEEE/CVF Conference on Computer Vision and Pattern Recognition*, pages 7108–7118, 2021.

[26] Jingwei Huang, Hao Su, and Leonidas Guibas. Robust watertight manifold surface generation method for shapenet models. *arXiv preprint arXiv:1802.01698*, 2018.

[27] Denys Iliash, Hanxiao Jiang, Yiming Zhang, Manolis Savva, and Angel X Chang. S2o: Static to openable enhancement for articulated 3d objects. *arXiv preprint arXiv:2409.18896*, 2024.

[28] Ajinkya Jain, Stephen Giguere, Rudolf Lioutikov, and Scott Niekum. Distributional depth-based estimation of object articulation models. In *Conference on Robot Learning*, pages 1611–1621. PMLR, 2022.

[29] Ajinkya Jain, Rudolf Lioutikov, Caleb Chuck, and Scott Niekum. Screwnet: Category-independent articulation model estimation from depth images using screw theory. In *2021 IEEE International Conference on Robotics and Automation (ICRA)*, pages 13670–13677. IEEE, 2021.

[30] Michael Joswig, Thorsten Theobald, Michael Joswig, and Thorsten Theobald. Plücker coordinates and lines in space. *Polyhedral and Algebraic Methods in Computational Geometry*, pages 193–207, 2013.

[31] Akash Abdu Jyothi, Thibaut Durand, Jiawei He, Leonid Sigal, and Greg Mori. Layoutvae: Stochastic scene layout generation from a label set. In *Proceedings of the IEEE/CVF International Conference on Computer Vision*, pages 9895–9904, 2019.

[32] Kamil Kamiński, Jan Ludwiczak, Maciej Jasiński, Adriana Bukala, Rafal Madaj, Krzysztof Szczepaniak, and Stanisław Dunin-Horkawicz. Rossmann-toolbox: a deep learning-based protocol for the prediction and design of cofactor specificity in rossmann fold proteins. *Briefings in bioinformatics*, 23(1):bbab371, 2022.

[33] Dov Katz and Oliver Brock. Manipulating articulated objects with interactive perception. In *2008 IEEE International Conference on Robotics and Automation*, pages 272–277. IEEE, 2008.

[34] Yuki Kawana, Yusuke Mukuta, and Tatsuya Harada. Unsupervised pose-aware part decomposition for man-made articulated objects. In *European Conference on Computer Vision*, pages 558–575. Springer, 2022.

[35] Juil Koo, Seungwoo Yoo, Minh Hieu Nguyen, and Minhyuk Sung. Salad: Part-level latent diffusion for 3d shape generation and manipulation. In *Proceedings of the IEEE/CVF International Conference on Computer Vision*, pages 14441–14451, 2023.

[36] Jiahui Lei, Congyue Deng, Karl Schmeckpeper, Leonidas Guibas, and Kostas Daniilidis. Efem: Equivariant neural field expectation maximization for 3d object segmentation without scene supervision. In *Proceedings of the IEEE/CVF Conference on Computer Vision and Pattern Recognition*, 2023.

[37] Jiahui Lei, Congyue Deng, Bokui Shen, Leonidas Guibas, and Kostas Daniilidis. Nap: Neural 3d articulated object prior. In *Thirty-seventh Conference on Neural Information Processing Systems*, 2023.

[38] Jianan Li, Jimei Yang, Aaron Hertzmann, Jianming Zhang, and Tingfa Xu. Layoutgan: Generating graphic layouts with wireframe discriminators. *arXiv preprint arXiv:1901.06767*, 2019.

[39] Muheng Li, Yueqi Duan, Jie Zhou, and Jiwen Lu. Diffusion-sdf: Text-to-shape via voxelized diffusion. In *Proceedings of the IEEE/CVF Conference on Computer Vision and Pattern Recognition*, pages 12642–12651, 2023.

[40] Tianye Li, Timo Bolkart, Michael J Black, Hao Li, and Javier Romero. Learning a model of facial shape and expression from 4d scans. *ACM Trans. Graph.*, 36(6):194–1, 2017.

[41] Xiaolong Li, He Wang, Li Yi, Leonidas J Guibas, A Lynn Abbott, and Shuran Song. Category-level articulated object pose estimation. In *Proceedings of the IEEE/CVF conference on computer vision and pattern recognition*, pages 3706–3715, 2020.

[42] Chen-Hsuan Lin, Jun Gao, Luming Tang, Towaki Takikawa, Xiaohui Zeng, Xun Huang, Karsten Kreis, Sanja Fidler, Ming-Yu Liu, and Tsung-Yi Lin. Magic3d: High-resolution text-to-3d content creation. In *Proceedings of the IEEE/CVF Conference on Computer Vision and Pattern Recognition*, pages 300–309, 2023.

[43] Gengxin Liu, Qian Sun, Haibin Huang, Chongyang Ma, Yulan Guo, Li Yi, Hui Huang, and Ruizhen Hu. Semi-weakly supervised object kinematic motion prediction. In *Proceedings of the IEEE/CVF Conference on Computer Vision and Pattern Recognition*, pages 21726–21735, 2023.

[44] Jiayi Liu, Ali Mahdavi-Amiri, and Manolis Savva. Paris: Part-level reconstruction and motion analysis for articulated objects. In *Proceedings of the IEEE/CVF International Conference on Computer Vision*, pages 352–363, 2023.

[45] Jiayi Liu, Manolis Savva, and Ali Mahdavi-Amiri. Survey on modeling of articulated objects. *arXiv preprint arXiv:2403.14937*, 2024.

[46] Jiayi Liu, Hou In Ivan Tam, Ali Mahdavi-Amiri, and Manolis Savva. Cage: Controllable articulation generation. In *Proceedings of the IEEE/CVF Conference on Computer Vision and Pattern Recognition*, pages 17880–17889, 2024.

[47] Liu Liu, Wenqiang Xu, Haoyuan Fu, Sucheng Qian, Qiaojun Yu, Yang Han, and Cewu Lu. Akb-48: A real-world articulated object knowledge base. In *Proceedings of the IEEE/CVF Conference on Computer Vision and Pattern Recognition*, pages 14809–14818, 2022.

[48] Minghua Liu, Ruoxi Shi, Linghao Chen, Zhuoyang Zhang, Chao Xu, Xinyue Wei, Hansheng Chen, Chong Zeng, Jiayuan Gu, and Hao Su. One-2-3-45++: Fast single image to 3d objects with consistent multi-view generation and 3d diffusion. *arXiv preprint arXiv:2311.07885*, 2023.

 https://doi.org/10.52202/079017-0050

[49] Qihao Liu, Weichao Qiu, Weiyao Wang, Gregory D Hager, and Alan L Yuille. Nothing but geometric constraints: A model-free method for articulated object pose estimation. *arXiv preprint arXiv:2012.00088*, 2020.

[50] Ruoshi Liu, Rundi Wu, Basile Van Hoorick, Pavel Tokmakov, Sergey Zakharov, and Carl Vondrick. Zero-1-to-3: Zero-shot one image to 3d object. In *Proceedings of the IEEE/CVF International Conference on Computer Vision*, pages 9298–9309, 2023.

[51] Xueyi Liu, Ji Zhang, Ruizhen Hu, Haibin Huang, He Wang, and Li Yi. Self-supervised category-level articulated object pose estimation with part-level se (3) equivariance. *arXiv preprint arXiv:2302.14268*, 2023.

[52] Zhen Liu, Yao Feng, Michael J Black, Derek Nowrouzezahrai, Liam Paull, and Weiyang Liu. Meshdiffusion: Score-based generative 3d mesh modeling. *arXiv preprint arXiv:2303.08133*, 2023.

[53] Zhengzhe Liu, Jingyu Hu, Ka-Hei Hui, Xiaojuan Qi, Daniel Cohen-Or, and Chi-Wing Fu. Exim: A hybrid explicit-implicit representation for text-guided 3d shape generation. *ACM Transactions on Graphics (TOG)*, 42(6):1–12, 2023.

[54] Xiaoxiao Long, Yuan-Chen Guo, Cheng Lin, Yuan Liu, Zhiyang Dou, Lingjie Liu, Yuexin Ma, Song-Hai Zhang, Marc Habermann, Christian Theobalt, et al. Wonder3d: Single image to 3d using cross-domain diffusion. *arXiv preprint arXiv:2310.15008*, 2023.

[55] Matthew Loper, Naureen Mahmood, Javier Romero, Gerard Pons-Moll, and Michael J Black. Smpl: A skinned multi-person linear model. In *Seminal Graphics Papers: Pushing the Boundaries, Volume 2*, pages 851–866, 2023.

[56] William E. Lorensen and Harvey E. Cline. Marching cubes: A high resolution 3d surface construction algorithm. In *SIGGRAPH*, pages 163–169. ACM, 1987.

[57] Jonathan Lorraine, Kevin Xie, Xiaohui Zeng, Chen-Hsuan Lin, Towaki Takikawa, Nicholas Sharp, Tsung-Yi Lin, Ming-Yu Liu, Sanja Fidler, and James Lucas. Att3d: Amortized text-to-3d object synthesis. In *Proceedings of the IEEE/CVF International Conference on Computer Vision*, pages 17946–17956, 2023.

[58] Rundong Luo, Haoran Geng, Congyue Deng, Puhao Li, Zan Wang, Baoxiong Jia, Leonidas Guibas, and Siyuang Huang. Physpart: Physically plausible part completion for interactable objects. *arXiv preprint arXiv:2408.13724*, 2024.

[59] Shitong Luo and Wei Hu. Diffusion probabilistic models for 3d point cloud generation. In *Proceedings of the IEEE/CVF Conference on Computer Vision and Pattern Recognition*, pages 2837–2845, 2021.

[60] Zhaoyang Lyu, Zhifeng Kong, Xudong Xu, Liang Pan, and Dahua Lin. A conditional point diffusion-refinement paradigm for 3d point cloud completion. *arXiv preprint arXiv:2112.03530*, 2021.

[61] Jing Ma and Dongliang Zhang. Tarig: Adaptive template-aware neural rigging for humanoid characters. *Computers & Graphics*, 114:158–167, 2023.

[62] Zhao Mandi, Yijia Weng, Dominik Bauer, and Shuran Song. Real2code: Reconstruct articulated objects via code generation. *arXiv preprint arXiv:2406.08474*, 2024.

[63] Yongsen Mao, Yiming Zhang, Hanxiao Jiang, Angel Chang, and Manolis Savva. Multiscan: Scalable rgbd scanning for 3d environments with articulated objects. *Advances in Neural Information Processing Systems*, 35:9058–9071, 2022.

[64] Roberto Martin Martin and Oliver Brock. Online interactive perception of articulated objects with multi-level recursive estimation based on task-specific priors. In *2014 IEEE/RSJ International Conference on Intelligent Robots and Systems*, pages 2494–2501. IEEE, 2014.

[65] Roberto Martín-Martín, Clemens Eppner, and Oliver Brock. The rbo dataset of articulated objects and interactions. *The International Journal of Robotics Research*, 38(9):1013–1019, 2019.

[66] Roberto Martín-Martín, Sebastian Höfer, and Oliver Brock. An integrated approach to visual perception of articulated objects. In *2016 IEEE international conference on robotics and automation (ICRA)*, pages 5091–5097. IEEE, 2016.

[67] Kaichun Mo, Leonidas J Guibas, Mustafa Mukadam, Abhinav Gupta, and Shubham Tulsiani. Where2act: From pixels to actions for articulated 3d objects. In *Proceedings of the IEEE/CVF International Conference on Computer Vision*, pages 6813–6823, 2021.

[68] George Kiyohiro Nakayama, Mikaela Angelina Uy, Jiahui Huang, Shi-Min Hu, Ke Li, and Leonidas Guibas. Difffacto: Controllable part-based 3d point cloud generation with cross diffusion. In *Proceedings of the IEEE/CVF International Conference on Computer Vision*, pages 14257–14267, 2023.

[69] Neil Nie, Samir Yitzhak Gadre, Kiana Ehsani, and Shuran Song. Structure from action: Learning interactions for articulated object 3d structure discovery. *arXiv preprint arXiv:2207.08997*, 2022.

[70] Stefan Novaković and Vladimir Risojević. Learning localization of body and finger animation skeleton joints on three-dimensional models of human bodies. In *2024 Zooming Innovation in Consumer Technologies Conference (ZINC)*, pages 19–24. IEEE, 2024.

[71] Despoina Paschalidou, Amlan Kar, Maria Shugrina, Karsten Kreis, Andreas Geiger, and Sanja Fidler. Atiss: Autoregressive transformers for indoor scene synthesis. *Advances in Neural Information Processing Systems*, 34:12013–12026, 2021.

[72] Akshay Gadi Patil, Supriya Gadi Patil, Manyi Li, Matthew Fisher, Manolis Savva, and Hao Zhang. Advances in data-driven analysis and synthesis of 3d indoor scenes. *arXiv preprint arXiv:2304.03188*, 2023.

[73] Ben Poole, Ajay Jain, Jonathan T Barron, and Ben Mildenhall. Dreamfusion: Text-to-3d using 2d diffusion. *arXiv preprint arXiv:2209.14988*, 2022.

[74] Guocheng Qian, Jinjie Mai, Abdullah Hamdi, Jian Ren, Aliaksandr Siarohin, Bing Li, Hsin-Ying Lee, Ivan Skorokhodov, Peter Wonka, Sergey Tulyakov, et al. Magic123: One image to high-quality 3d object generation using both 2d and 3d diffusion priors. *arXiv preprint arXiv:2306.17843*, 2023.

[75] Xuanchi Ren, Jiahui Huang, Xiaohui Zeng, Ken Museth, Sanja Fidler, and Francis Williams. Xcube (χ^3): Large-scale 3d generative modeling using sparse voxel hierarchies. *arXiv preprint arXiv:2312.03806*, 2023.

[76] Xuanchi Ren, Jiahui Huang, Xiaohui Zeng, Ken Museth, Sanja Fidler, and Francis Williams. Xcube: Large-scale 3d generative modeling using sparse voxel hierarchies. In *Proceedings of the IEEE/CVF Conference on Computer Vision and Pattern Recognition*, pages 4209–4219, 2024.

[77] Yichun Shi, Peng Wang, Jianglong Ye, Mai Long, Kejie Li, and Xiao Yang. Mvdream: Multi-view diffusion for 3d generation. *arXiv preprint arXiv:2308.16512*, 2023.

[78] Yawar Siddiqui, Antonio Alliegro, Alexey Artemov, Tatiana Tommasi, Daniele Sirigatti, Vladislav Rosov, Angela Dai, and Matthias Nießner. Meshgpt: Generating triangle meshes with decoder-only transformers. *arXiv preprint arXiv:2311.15475*, 2023.

[79] Jascha Sohl-Dickstein, Eric Weiss, Niru Maheswaranathan, and Surya Ganguli. Deep unsupervised learning using nonequilibrium thermodynamics. In *International conference on machine learning*, pages 2256–2265. PMLR, 2015.

[80] Jiaming Song, Chenlin Meng, and Stefano Ermon. Denoising diffusion implicit models. *arXiv preprint arXiv:2010.02502*, 2020.

[81] Jürgen Sturm, Christian Plagemann, and Wolfram Burgard. Adaptive body scheme models for robust robotic manipulation. In *Robotics: Science and systems*. Zurich, 2008.

 https://doi.org/10.52202/079017-0050

[82] Jurgen Sturm, Christian Plagemann, and Wolfram Burgard. Unsupervised body scheme learning through self-perception. In *2008 IEEE International Conference on Robotics and Automation*, pages 3328–3333. IEEE, 2008.

[83] Jürgen Sturm, Cyrill Stachniss, and Wolfram Burgard. A probabilistic framework for learning kinematic models of articulated objects. *Journal of Artificial Intelligence Research*, 41:477–526, 2011.

[84] Jiapeng Tang, Yinyu Nie, Lev Markhasin, Angela Dai, Justus Thies, and Matthias Nießner. Diffuscene: Scene graph denoising diffusion probabilistic model for generative indoor scene synthesis. *arXiv preprint arXiv:2303.14207*, 2023.

[85] Jiaxiang Tang, Jiawei Ren, Hang Zhou, Ziwei Liu, and Gang Zeng. Dreamgaussian: Generative gaussian splatting for efficient 3d content creation. *arXiv preprint arXiv:2309.16653*, 2023.

[86] Emanuel Todorov, Tom Erez, and Yuval Tassa. Mujoco: A physics engine for model-based control. In *2012 IEEE/RSJ international conference on intelligent robots and systems*, pages 5026–5033. IEEE, 2012.

[87] J ürgen Sturm, Vijay Pradeep, Cyrill Stachniss, Christian Plagemann, Kurt Konolige, and Wolfram Burgard. Learning kinematic models for articulated objects. In *Twenty-First International Joint Conference on Artificial Intelligence*. Citeseer, 2009.

[88] Arash Vahdat, Francis Williams, Zan Gojcic, Or Litany, Sanja Fidler, Karsten Kreis, et al. Lion: Latent point diffusion models for 3d shape generation. *Advances in Neural Information Processing Systems*, 35:10021–10039, 2022.

[89] Aaron Van Den Oord, Oriol Vinyals, et al. Neural discrete representation learning. *Advances in neural information processing systems*, 30, 2017.

[90] Petar Veličković, Guillem Cucurull, Arantxa Casanova, Adriana Romero, Pietro Lio, and Yoshua Bengio. Graph attention networks. *arXiv preprint arXiv:1710.10903*, 2017.

[91] Clement Vignac, Nagham Osman, Laura Toni, and Pascal Frossard. Midi: Mixed graph and 3d denoising diffusion for molecule generation. *arXiv preprint arXiv:2302.09048*, 2023.

[92] Xiaogang Wang, Bin Zhou, Yahao Shi, Xiaowu Chen, Qinping Zhao, and Kai Xu. Shape2motion: Joint analysis of motion parts and attributes from 3d shapes. In *Proceedings of the IEEE/CVF Conference on Computer Vision and Pattern Recognition*, pages 8876–8884, 2019.

[93] Zhengyi Wang, Cheng Lu, Yikai Wang, Fan Bao, Chongxuan Li, Hang Su, and Jun Zhu. Prolificdreamer: High-fidelity and diverse text-to-3d generation with variational score distillation. *Advances in Neural Information Processing Systems*, 36, 2024.

[94] Yijia Weng, He Wang, Qiang Zhou, Yuzhe Qin, Yueqi Duan, Qingnan Fan, Baoquan Chen, Hao Su, and Leonidas J Guibas. Captra: Category-level pose tracking for rigid and articulated objects from point clouds. In *Proceedings of the IEEE/CVF International Conference on Computer Vision*, pages 13209–13218, 2021.

[95] Qianyi Wu, Kaisiyuan Wang, Kejie Li, Jianmin Zheng, and Jianfei Cai. Objectsdf++: Improved object-compositional neural implicit surfaces. In *Proceedings of the IEEE/CVF International Conference on Computer Vision*, pages 21764–21774, 2023.

[96] Ruihai Wu, Yan Zhao, Kaichun Mo, Zizheng Guo, Yian Wang, Tianhao Wu, Qingnan Fan, Xuelin Chen, Leonidas Guibas, and Hao Dong. Vat-mart: Learning visual action trajectory proposals for manipulating 3d articulated objects. *arXiv preprint arXiv:2106.14440*, 2021.

[97] Fanbo Xiang, Yuzhe Qin, Kaichun Mo, Yikuan Xia, Hao Zhu, Fangchen Liu, Minghua Liu, Hanxiao Jiang, Yifu Yuan, He Wang, et al. Sapien: A simulated part-based interactive environment. In *Proceedings of the IEEE/CVF Conference on Computer Vision and Pattern Recognition*, pages 11097–11107, 2020.

[98] Jiale Xu, Xintao Wang, Weihao Cheng, Yan-Pei Cao, Ying Shan, Xiaohu Qie, and Shenghua Gao. Dream3d: Zero-shot text-to-3d synthesis using 3d shape prior and text-to-image diffusion models. In *Proceedings of the IEEE/CVF Conference on Computer Vision and Pattern Recognition*, pages 20908–20918, 2023.

[99] Xianghao Xu, Yifan Ruan, Srinath Sridhar, and Daniel Ritchie. Unsupervised kinematic motion detection for part-segmented 3d shape collections. In *ACM SIGGRAPH 2022 Conference Proceedings*, pages 1–9, 2022.

[100] Zhan Xu, Yang Zhou, Evangelos Kalogerakis, Chris Landreth, and Karan Singh. Rignet: Neural rigging for articulated characters. *arXiv preprint arXiv:2005.00559*, 2020.

[101] Zhan Xu, Yang Zhou, Li Yi, and Evangelos Kalogerakis. Morig: Motion-aware rigging of character meshes from point clouds. In *SIGGRAPH Asia 2022 conference papers*, pages 1–9, 2022.

[102] Zihao Yan, Ruizhen Hu, Xingguang Yan, Luanmin Chen, Oliver Van Kaick, Hao Zhang, and Hui Huang. Rpm-net: recurrent prediction of motion and parts from point cloud. *arXiv preprint arXiv:2006.14865*, 2020.

[103] Jianglong Ye, Peng Wang, Kejie Li, Yichun Shi, and Heng Wang. Consistent-1-to-3: Consistent image to 3d view synthesis via geometry-aware diffusion models. *arXiv preprint arXiv:2310.03020*, 2023.

[104] Li Yi, Haibin Huang, Difan Liu, Evangelos Kalogerakis, Hao Su, and Leonidas Guibas. Deep part induction from articulated object pairs. *arXiv preprint arXiv:1809.07417*, 2018.

[105] Qiaojun Yu, Junbo Wang, Wenhai Liu, Ce Hao, Liu Liu, Lin Shao, Weiming Wang, and Cewu Lu. Gamma: Generalizable articulation modeling and manipulation for articulated objects. *arXiv preprint arXiv:2309.16264*, 2023.

[106] Vicky Zeng, Tabitha Edith Lee, Jacky Liang, and Oliver Kroemer. Visual identification of articulated object parts. In *2021 IEEE/RSJ International Conference on Intelligent Robots and Systems (IROS)*, pages 2443–2450. IEEE, 2021.

[107] Guangyao Zhai, Evin Pinar Örnek, Shun-Cheng Wu, Yan Di, Federico Tombari, Nassir Navab, and Benjamin Busam. Commonscenes: Generating commonsense 3d indoor scenes with scene graphs. *arXiv preprint arXiv:2305.16283*, 2023.

[108] Biao Zhang, Jiapeng Tang, Matthias Niessner, and Peter Wonka. 3dshape2vecset: A 3d shape representation for neural fields and generative diffusion models. *ACM Transactions on Graphics (TOG)*, 42(4):1–16, 2023.

[109] Li Zhang, Zean Han, Yan Zhong, Qiaojun Yu, Xingyu Wu, et al. Vocapter: Voting-based pose tracking for category-level articulated object via inter-frame priors. In *ACM Multimedia 2024*, 2024.

[110] Longwen Zhang, Ziyu Wang, Qixuan Zhang, Qiwei Qiu, Anqi Pang, Haoran Jiang, Wei Yang, Lan Xu, and Jingyi Yu. Clay: A controllable large-scale generative model for creating high-quality 3d assets. *arXiv preprint arXiv:2406.13897*, 2024.

[111] Xin-Yang Zheng, Hao Pan, Peng-Shuai Wang, Xin Tong, Yang Liu, and Heung-Yeung Shum. Locally attentional sdf diffusion for controllable 3d shape generation. *arXiv preprint arXiv:2305.04461*, 2023.

[112] Chenliang Zhou, Fangcheng Zhong, Param Hanji, Zhilin Guo, Kyle Fogarty, Alejandro Sztrajman, Hongyun Gao, and Cengiz Oztireli. Frepolad: Frequency-rectified point latent diffusion for point cloud generation. *arXiv preprint arXiv:2311.12090*, 2023.

[113] Linqi Zhou, Yilun Du, and Jiajun Wu. 3d shape generation and completion through point-voxel diffusion. In *Proceedings of the IEEE/CVF International Conference on Computer Vision*, pages 5826–5835, 2021.

[114] Silvia Zuffi, Angjoo Kanazawa, David W Jacobs, and Michael J Black. 3d menagerie: Modeling the 3d shape and pose of animals. In *Proceedings of the IEEE conference on computer vision and pattern recognition*, pages 6365–6373, 2017.

 https://doi.org/10.52202/079017-0050

A Details of the Training and Inference Process

A.1 Training and Inference of the Structure Generator

As highlighted in [37, 46], the different characteristics of an articulated asset can be represented as features of a complete graph $\boldsymbol{G}_N = \{\boldsymbol{x}, \boldsymbol{e}\}_N$ with N nodes, and $N(N-1)/2$ edges. We train an image VQVAE [89] using different views of every single object of the dataset. The latent code of every object i composing an articulated asset is of dimension 8×8. This latent code is vectorized in an array $\boldsymbol{f}_i \in \mathbb{R}^{64}$ before being concatenated to the reference node feature vector $\boldsymbol{x}_i$ (see Figure 6).

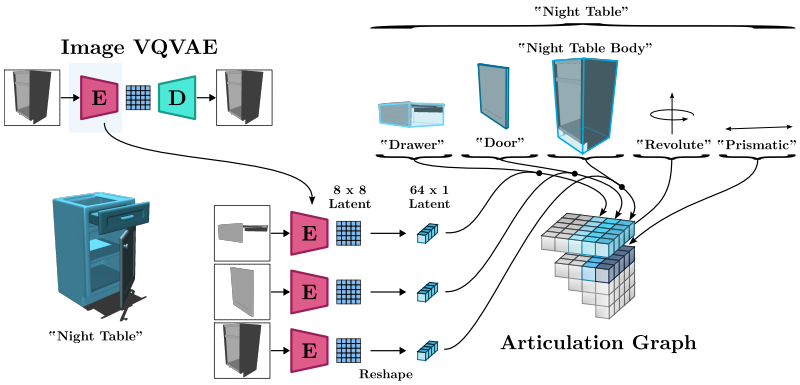

Figure 6: Detail of the structure generation training pipeline.

The node and edge features of the obtained asset graph $\boldsymbol{G}_N$ are then iteratively corrupted by Gaussian noise that a Graph ATtention network (GAT) learns to predict (see Figure 7).

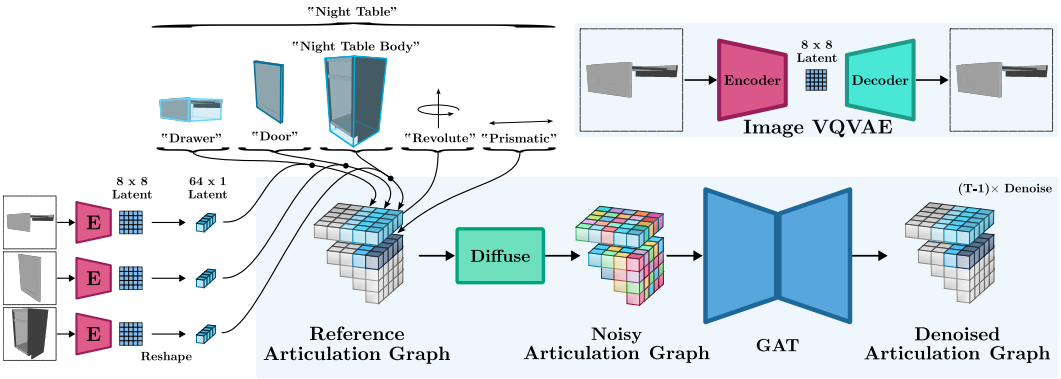

Figure 7: Detail of the structure generation training pipeline.

The denoised graph $\hat{\boldsymbol{G}}_N$ obtained at the output of the pipeline can then be post-processed into a *human interpretable* form, the node, joint and asset categorical information being converted into text while the denoised image latents $\boldsymbol{f}_i$ of every node i are decoded into corresponding images. This human interpretable content can then be passed as a condition signal to the shape generator (see Figure 8).

A.2 Denoising Diffusion Probabilistic Model (DDPM)

A.2.1 Forward Process

Given a sample $\boldsymbol{x}_0$ drawn from a distribution $q(\boldsymbol{x}_0)$, a series of noisy samples $\boldsymbol{x}_t, \forall t \in [1, \cdots, T]$ can be obtained by gradually corrupting $\boldsymbol{x}_0$ with Gaussian noise $\boldsymbol{\varepsilon} \sim \mathcal{N}(\boldsymbol{0}, \boldsymbol{I})$ following a variance schedule $\beta_1 < \cdots < \beta_T$:

$$q(\boldsymbol{x}_{1:T}|\boldsymbol{x}_0) := \prod_{t=1}^{T} q(\boldsymbol{x}_t|\boldsymbol{x}_{t-1}), \quad q(\boldsymbol{x}_t|\boldsymbol{x}_{t-1}) := \mathcal{N}\left(\sqrt{1-\beta_t}\boldsymbol{x}_{t-1}, \beta_t \boldsymbol{I}\right). \tag{4}$$

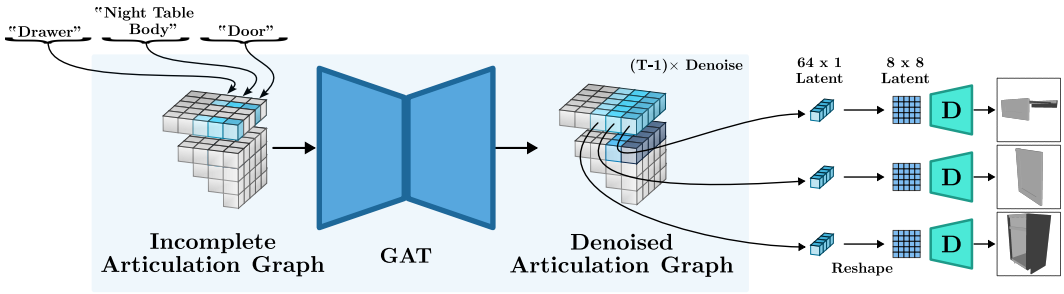

Figure 8: Detail of the structure generation inference pipeline.

A relevant property of such a diffusion process is that $\boldsymbol{x}_t$ can be sampled from $\boldsymbol{x}_0$ through

$$q(\boldsymbol{x}_t|\boldsymbol{x}_0) = \mathcal{N}(\sqrt{\bar{\alpha}_t}\boldsymbol{x}_0, (1-\bar{\alpha}_t)\,\boldsymbol{I}), \tag{5}$$

where $\alpha_t := 1 - \beta_t$ and $\bar{\alpha}_t = \prod_{s=1}^{t} \alpha_s$, eventually yielding $\boldsymbol{x}_t = \sqrt{\bar{\alpha}_t}\boldsymbol{x}_0 + \sqrt{1-\bar{\alpha}_t}\boldsymbol{\varepsilon}$.

A.2.2 Reverse Process.

Initiating from a standard Gaussian distribution, $\boldsymbol{x}_T \sim \mathcal{N}(0, \boldsymbol{I})$, a denoising model p_θ parameterized by trainable weights θ, learns to approximate a series of Gaussian transitions $p_\theta\left(\boldsymbol{x}_{t-1}|\boldsymbol{x}_t\right)$. These transitions incrementally denoise the signal such that

$$p_\theta\left(\boldsymbol{x}_{0:T}\right) \quad := \quad p_\theta\left(\boldsymbol{x}_T\right) \prod_{t=1}^{T} p_\theta\left(\boldsymbol{x}_{t-1}|\boldsymbol{x}_t\right), \tag{6}$$

$$p_\theta\left(\boldsymbol{x}_{t-1}|\boldsymbol{x}_t\right) \quad := \quad \mathcal{N}\left(\boldsymbol{\mu}_\theta\left(\boldsymbol{x}_t, t\right), \boldsymbol{\Sigma}_\theta\left(\boldsymbol{x}_t, t\right)\right). \tag{7}$$

Following the approach from [21], previous work on articulated asset generation [37] [46] define $\boldsymbol{\mu}_\theta = \frac{1}{\sqrt{\alpha_t}}\left(\boldsymbol{x}_t - \frac{\beta_t}{\sqrt{1-\bar{\alpha}_t}}\boldsymbol{\varepsilon}_\theta\left(\boldsymbol{x}_t, t\right)\right)$ and $\boldsymbol{\Sigma}_\theta(\boldsymbol{x}_t, t) = \sigma_t^2 \boldsymbol{I}$ yielding the following Langevin dynamics

$$\boldsymbol{x}_{t-1} = \frac{1}{\sqrt{\alpha_t}}\left(\boldsymbol{x}_t - \frac{\beta_t}{\sqrt{1-\bar{\alpha}_t}}\boldsymbol{\varepsilon}_\theta\left(\boldsymbol{x}_t, t\right)\right) + \sigma_t \boldsymbol{z}, \quad \boldsymbol{z} \sim \mathcal{N}\left(\boldsymbol{0}, \boldsymbol{I}\right), \tag{8}$$

where $\boldsymbol{\varepsilon}_\theta\left(\boldsymbol{x}_t, t\right)$ is a learnable network approximating the per-step noise on $\boldsymbol{x}_t$.

A.2.3 Loss Function

The variational lower bound is used to optimize the negative log-likelihood. Following the simplified training objective outlined in DDPM [21], the training loss can be simplified to the following expression

$$\mathcal{L} = \mathbb{E}_{\boldsymbol{x}_0, \boldsymbol{\varepsilon}_t}\left[\left\|\boldsymbol{\varepsilon}_t - \boldsymbol{\varepsilon}_\theta\left(\sqrt{\alpha_t}\boldsymbol{x}_0 + \sqrt{1-\bar{\alpha}_t}\boldsymbol{\varepsilon}_t, t\right)\right\|^2\right]. \tag{9}$$

https://doi.org/10.52202/079017-0050

B Data Preprocessing

B.1 Mesh Preprocessing

High-quality meshes are essential for applications such as generating Truncated Signed Distance Functions (TSDFs), which are in turn widely used within advanced 3D latent diffusion models such as SDFusion [8]. However, many meshes in popular datasets, including PartNet-Mobility [97], contain inconsistencies and errors that render them unsuitable for such purposes. To address these issues, we incorporate a preprocessing routine that includes a manifoldization process [26] to repair and convert flawed meshes into watertight, manifold counterparts (see Figure 9).

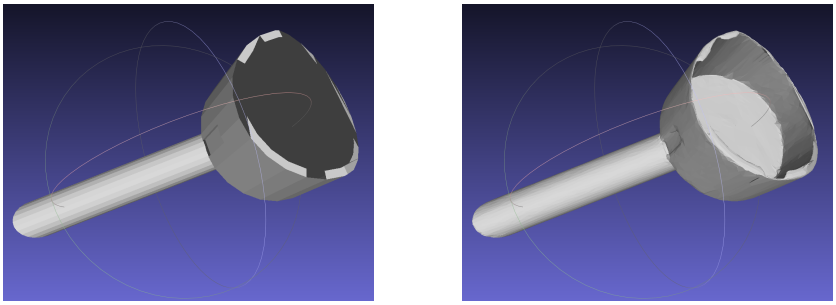

(a) Original mesh with inconsistencies (b) Repaired watertight manifold mesh

Figure 9: Mesh repair pipeline: (a) The original mesh exhibits holes and non-manifold edges; (b) After preprocessing, the mesh is converted into a watertight manifold suitable for TSDF generation.

B.2 Orientation Estimation and OBB Computation

Unlike previous approaches [37, 46], we do not assume that the dataset meshes are already provided in a canonical orientation. Our method hence involves an orientation estimation process for each individual mesh, performed through the calculation of its Oriented Bounding Box (OBB). This OBB is subsequently utilized to align each body into a standard pose. The orientation estimation begins by

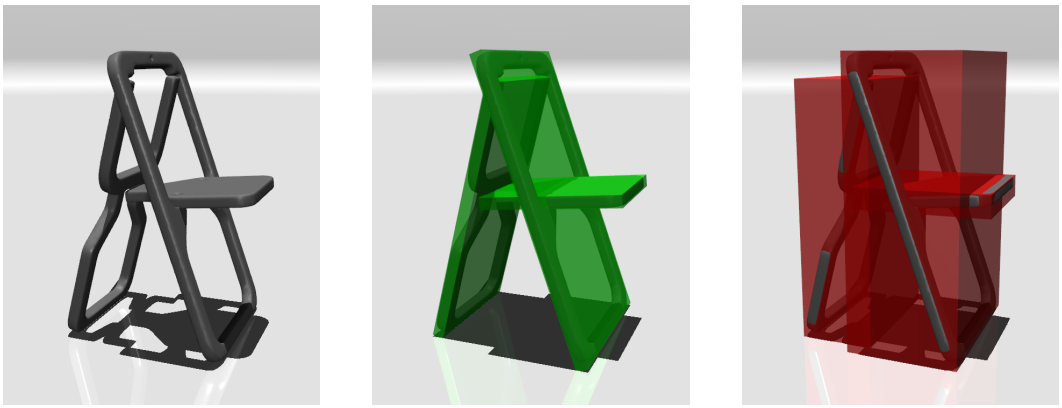

(a) Original mesh (b) Mesh with computed OBBs (c) Mesh with original AABBs

Figure 10: Comparison of bounding boxes: (a) The original mesh; (b) The mesh enclosed by Oriented Bounding Boxes (OBBs), providing a tight and accurate fit; (c) The mesh enclosed by original Axis-Aligned Bounding Boxes (AABBs).

applying Principal Component Analysis (PCA) to the mesh data. To mitigate the influence of complex internal geometries, such as shelves within furniture models, we first compute the convex hull of the mesh. This step simplifies the geometry while preserving the overall shape. We then voxelize the convex hull and uniformly sample 10,000 volumetric points from it. Applying PCA to these sampled points provides an initial estimate of the mesh's principal axes and orientation. Building upon this

initial estimate, we refine the attitude quaternion of the OBB through gradient descent optimization. The objective is to minimize the volume of the OBB, achieving a tighter fit around the mesh. During optimization, we iteratively adjust the orientation by recalculating the OBB volume along the oriented principal axes. To reliably navigate the solution space and avoid local minima, we incorporate a heuristic that explores potential orientations within a cone defined by an angle θ centered around the current best estimate. This approach allows for nuanced adjustments and aids in converging to a global minimum, thereby enhancing the precision of the orientation estimation. By combining PCA for initial alignment with heuristic-augmented gradient descent for volume minimization, our method ensures accurate and robust alignment of dataset meshes into their canonical poses (see Figure 10). This preprocessing step significantly enhances the overall quality and consistency of the articulated objects generated by our framework.

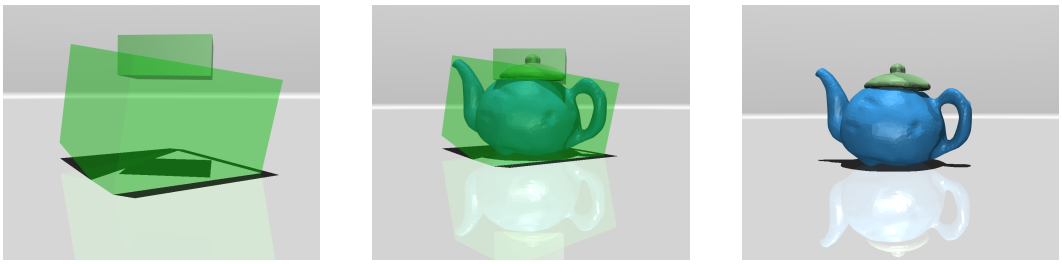

(a) Oriented Bounding Boxes

(b) Generated asset with Oriented Bounding Boxes

(c) Generated asset

Figure 11: An articulated asset simulated in the MuJoCo[86] physics engine.

C Controlling Generation with Asset Labels

MIDGArD incorporates categorical embeddings for asset types and object categories directly into the node features of the articulation graph. These embeddings enable the model to understand and generate objects that belong to a specified category, capturing the common structural and kinematic features associated with that category. The model is trained on a diverse dataset that includes various object categories with different articulation patterns. By learning statistical priors over these categories, MIDGArD can infer plausible structures and motions for new objects within the same category. The structure generator is designed to handle incomplete or partial inputs, allowing it to fill in missing details based on learned patterns. In the absence of detailed node-level information, the model can perform unconditional generation, producing coherent articulation graphs solely based on the provided asset category. The use of categorical embeddings and latent codes that correspond to human-understandable concepts (like “storage furniture”) makes it easier for users to interact with and guide the generation process.

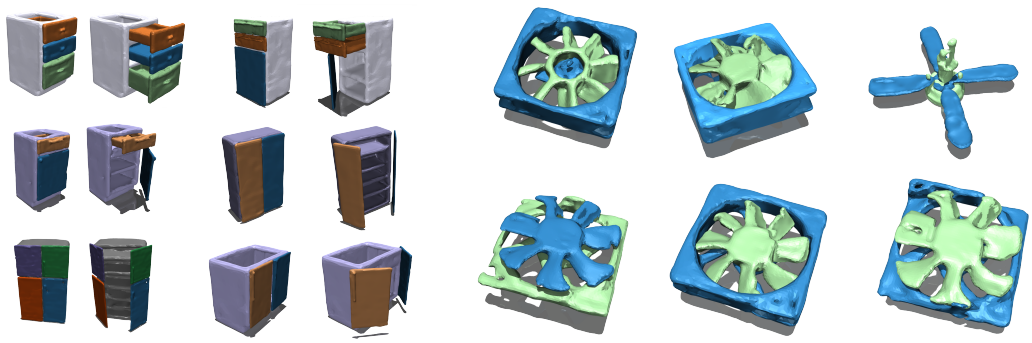

(a) Controlled generations with asset label "storage furniture"

(b) Controlled generations with asset label "fan"

Figure 12: Controlled Generation with Asset Labels.

https://doi.org/10.52202/079017-0050

D Controlling Generation with Image Input

A key advantage of MIDGArD's modular setup is the controllability of the generative process, not only on a graph level (by supplying partial graphs) but also on a part-level, by replacing the generated image or text information. In Figure 13, we provide examples how modifying the input image to the shape generator (SDFusion) changes the object appearance. Here, we randomly choose images from PartNet Mobility, sampling among all parts with the same category. For example, we sample from from all meshes with the descriptions "*A wheel as part of a cart*" to generate the wheel in the fifth row of Figure 13.

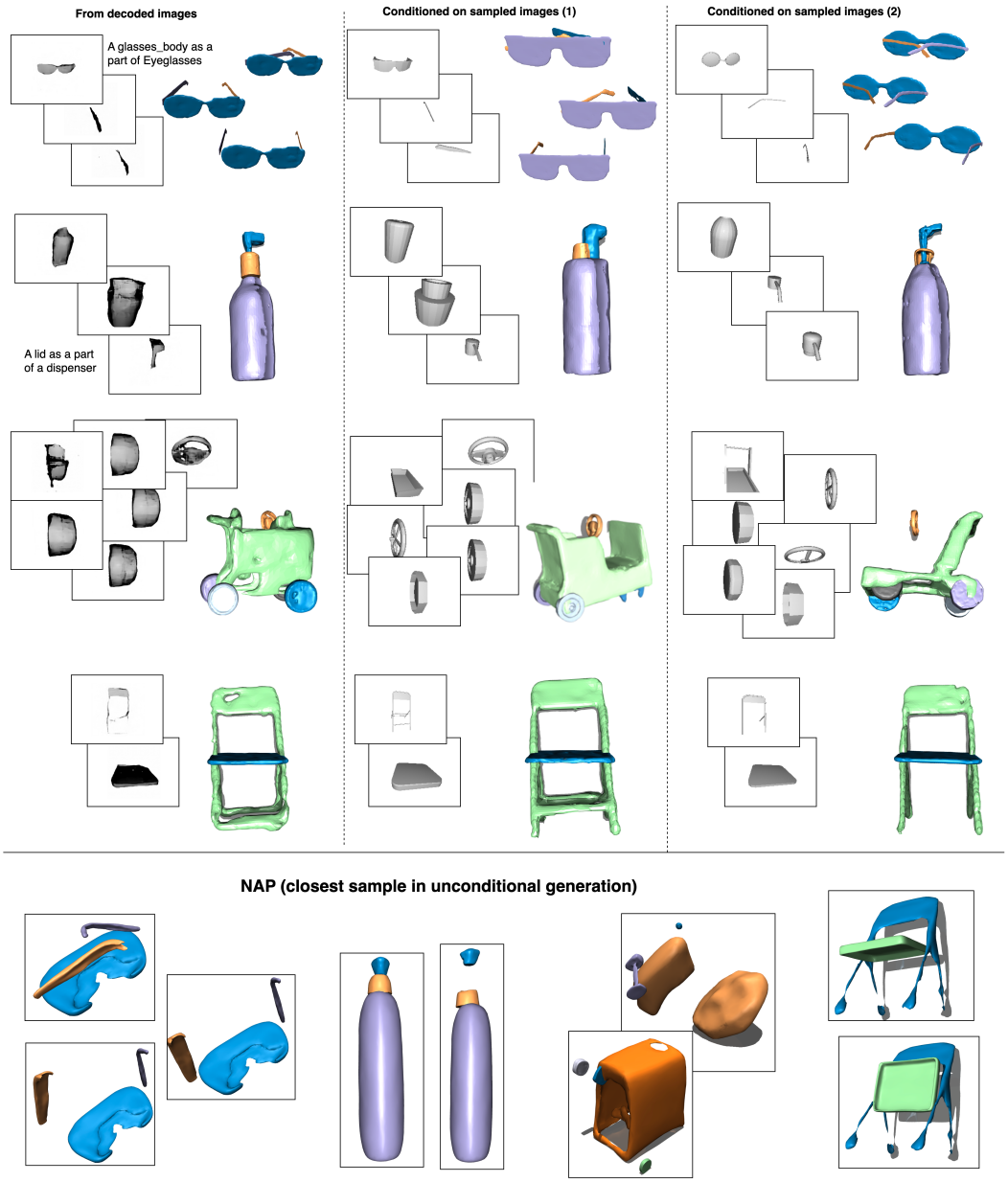

Figure 13: Controlling the shape appearance of object parts via image conditioning. Top: Image inputs allow to control the object design on a part-level. Bottom: NAP struggles to generate objects with many parts and yields unrealistic motion.

https://doi.org/10.52202/079017-0050

E Encoding object-level information with Graph Attention Networks

For capturing the relationships between parts, we experiment with graph encodings as input to the conditional shape generation process. To generate the geometry for a specific part ϕ, we construct a simplified graph from the articulation graph that provides information about the size of the ϕ in comparison to other parts, as well as the joints between ϕ and other parts. Specifically, let $G_\phi = (\boldsymbol{v}_\phi, \boldsymbol{e}_\phi)$ be a graph with t_i as the node feature vector for the i-th node and the Plücker coordinates p_{ij} serving as edge features. We test two options to mark ϕ as the part to be generated: (1) a tree structure where $\boldsymbol{v}_{phi}$ is constructed by reducing the graph to the parts adjacent to ϕ, and (2) a complete graph ($\boldsymbol{v}_\phi = \boldsymbol{v}$) where the node features are augmented with a binary indicator that equals 1 for the node representing ϕ. These structures are processed with a Graph Attention Network (GAT), which is trained concurrently with the diffusion model. As shown in Table 4, the results do not match the ones of a simple MLP embedding, neither with nor without our *bb prior* method. We hypothesize that this is due to concurrently training the GAT with the diffusion model, possibly converging slower than an MLP. Furthermore, many objects in PartNet Mobility have few parts, leading to small graphs of less than 4 nodes. Future work could try to pretrain a GAT on graph-encoding to improve the conditional generation with object-level information.

Table 4: Shape generation results contrasting an MLP-based embedding to a GAT encoder.

	OBB_{count}	OBB_{sum}	CD (generated)	CD (scaled)
bb prior + bb MLP	1146	10.89	0.0072	0.0043
bb prior + tree GAT	1246	10.97	0.0076	0.0044
bb prior + graph GAT	1226	13.12	0.0084	0.0046
original + bb MLP + oriented dataset	1490	37.15	0.0152	0.0061
original + oriented dataset + tree GAT	1994	69.66	0.0203	0.0051
original + oriented dataset + graph GAT	1710	49.42	0.0218	0.0052
original + bb MLP	3795	183.5	0.0307	0.008

https://doi.org/10.52202/079017-0050

NeurIPS Paper Checklist

1. **Claims**

   Question: Do the main claims made in the abstract and introduction accurately reflect the paper's contributions and scope?

   Answer: [Yes]

   Justification: The main claims are support by detailed results, comparison to State of the Art, open-source code upon acceptance, explicit mention of limitations, and a detailed method section, and thorough steps to reproduce our results.

   Guidelines:

   - The answer NA means that the abstract and introduction do not include the claims made in the paper.
   - The abstract and/or introduction should clearly state the claims made, including the contributions made in the paper and important assumptions and limitations. A No or NA answer to this question will not be perceived well by the reviewers.
   - The claims made should match theoretical and experimental results, and reflect how much the results can be expected to generalize to other settings.
   - It is fine to include aspirational goals as motivation as long as it is clear that these goals are not attained by the paper.

2. **Limitations**

   Question: Does the paper discuss the limitations of the work performed by the authors?

   Answer: [Yes]

   Justification: please find our limitations of the work in the Conclusion section.

   Guidelines:

   - The answer NA means that the paper has no limitation while the answer No means that the paper has limitations, but those are not discussed in the paper.
   - The authors are encouraged to create a separate "Limitations" section in their paper.
   - The paper should point out any strong assumptions and how robust the results are to violations of these assumptions (e.g., independence assumptions, noiseless settings, model well-specification, asymptotic approximations only holding locally). The authors should reflect on how these assumptions might be violated in practice and what the implications would be.
   - The authors should reflect on the scope of the claims made, e.g., if the approach was only tested on a few datasets or with a few runs. In general, empirical results often depend on implicit assumptions, which should be articulated.
   - The authors should reflect on the factors that influence the performance of the approach. For example, a facial recognition algorithm may perform poorly when image resolution is low or images are taken in low lighting. Or a speech-to-text system might not be used reliably to provide closed captions for online lectures because it fails to handle technical jargon.
   - The authors should discuss the computational efficiency of the proposed algorithms and how they scale with dataset size.
   - If applicable, the authors should discuss possible limitations of their approach to address problems of privacy and fairness.
   - While the authors might fear that complete honesty about limitations might be used by reviewers as grounds for rejection, a worse outcome might be that reviewers discover limitations that aren't acknowledged in the paper. The authors should use their best judgment and recognize that individual actions in favor of transparency play an important role in developing norms that preserve the integrity of the community. Reviewers will be specifically instructed to not penalize honesty concerning limitations.

3. **Theory Assumptions and Proofs**

   Question: For each theoretical result, does the paper provide the full set of assumptions and a complete (and correct) proof?

Answer: [NA]

Justification: This work das not include theoretical results, proofs, or theorems.

Guidelines:

- The answer NA means that the paper does not include theoretical results.
- All the theorems, formulas, and proofs in the paper should be numbered and cross-referenced.
- All assumptions should be clearly stated or referenced in the statement of any theorems.
- The proofs can either appear in the main paper or the supplemental material, but if they appear in the supplemental material, the authors are encouraged to provide a short proof sketch to provide intuition.
- Inversely, any informal proof provided in the core of the paper should be complemented by formal proofs provided in appendix or supplemental material.
- Theorems and Lemmas that the proof relies upon should be properly referenced.

4. **Experimental Result Reproducibility**

   Question: Does the paper fully disclose all the information needed to reproduce the main experimental results of the paper to the extent that it affects the main claims and/or conclusions of the paper (regardless of whether the code and data are provided or not)?

   Answer: [Yes]

   Justification: we rigorously outlined the dataset, training method, implementation detail in the Result section and will enable reproducibility of results through open-source code upon acceptance.

   Guidelines:

   - The answer NA means that the paper does not include experiments.
   - If the paper includes experiments, a No answer to this question will not be perceived well by the reviewers: Making the paper reproducible is important, regardless of whether the code and data are provided or not.
   - If the contribution is a dataset and/or model, the authors should describe the steps taken to make their results reproducible or verifiable.
   - Depending on the contribution, reproducibility can be accomplished in various ways. For example, if the contribution is a novel architecture, describing the architecture fully might suffice, or if the contribution is a specific model and empirical evaluation, it may be necessary to either make it possible for others to replicate the model with the same dataset, or provide access to the model. In general. releasing code and data is often one good way to accomplish this, but reproducibility can also be provided via detailed instructions for how to replicate the results, access to a hosted model (e.g., in the case of a large language model), releasing of a model checkpoint, or other means that are appropriate to the research performed.
   - While NeurIPS does not require releasing code, the conference does require all submissions to provide some reasonable avenue for reproducibility, which may depend on the nature of the contribution. For example
     (a) If the contribution is primarily a new algorithm, the paper should make it clear how to reproduce that algorithm.
     (b) If the contribution is primarily a new model architecture, the paper should describe the architecture clearly and fully.
     (c) If the contribution is a new model (e.g., a large language model), then there should either be a way to access this model for reproducing the results or a way to reproduce the model (e.g., with an open-source dataset or instructions for how to construct the dataset).
     (d) We recognize that reproducibility may be tricky in some cases, in which case authors are welcome to describe the particular way they provide for reproducibility. In the case of closed-source models, it may be that access to the model is limited in some way (e.g., to registered users), but it should be possible for other researchers to have some path to reproducing or verifying the results.

5. **Open access to data and code**

https://doi.org/10.52202/079017-0050

Question: Does the paper provide open access to the data and code, with sufficient instructions to faithfully reproduce the main experimental results, as described in supplemental material?

Answer: [Yes]

Justification: Data of the results is provided at https://quentin-leboutet.github.io/MIDGArD/. Opensource code will be provided upon acceptance.

Guidelines:

- The answer NA means that paper does not include experiments requiring code.
- Please see the NeurIPS code and data submission guidelines (https://nips.cc/public/guides/CodeSubmissionPolicy) for more details.
- While we encourage the release of code and data, we understand that this might not be possible, so "No" is an acceptable answer. Papers cannot be rejected simply for not including code, unless this is central to the contribution (e.g., for a new open-source benchmark).
- The instructions should contain the exact command and environment needed to run to reproduce the results. See the NeurIPS code and data submission guidelines (https://nips.cc/public/guides/CodeSubmissionPolicy) for more details.
- The authors should provide instructions on data access and preparation, including how to access the raw data, preprocessed data, intermediate data, and generated data, etc.
- The authors should provide scripts to reproduce all experimental results for the new proposed method and baselines. If only a subset of experiments are reproducible, they should state which ones are omitted from the script and why.
- At submission time, to preserve anonymity, the authors should release anonymized versions (if applicable).
- Providing as much information as possible in supplemental material (appended to the paper) is recommended, but including URLs to data and code is permitted.

6. **Experimental Setting/Details**

Question: Does the paper specify all the training and test details (e.g., data splits, hyperparameters, how they were chosen, type of optimizer, etc.) necessary to understand the results?

Answer: [Yes]

Justification: we rigorously outlined the dataset, training method, implementation detail in the Result section and will enable reproducibility of results through open-source code upon acceptance.

Guidelines:

- The answer NA means that the paper does not include experiments.
- The experimental setting should be presented in the core of the paper to a level of detail that is necessary to appreciate the results and make sense of them.
- The full details can be provided either with the code, in appendix, or as supplemental material.

7. **Experiment Statistical Significance**

Question: Does the paper report error bars suitably and correctly defined or other appropriate information about the statistical significance of the experiments?

Answer: [NA]

Justification: no experiments that produce error bars or similar.

Guidelines:

- The answer NA means that the paper does not include experiments.
- The authors should answer "Yes" if the results are accompanied by error bars, confidence intervals, or statistical significance tests, at least for the experiments that support the main claims of the paper.

- The factors of variability that the error bars are capturing should be clearly stated (for example, train/test split, initialization, random drawing of some parameter, or overall run with given experimental conditions).
- The method for calculating the error bars should be explained (closed form formula, call to a library function, bootstrap, etc.)
- The assumptions made should be given (e.g., Normally distributed errors).
- It should be clear whether the error bar is the standard deviation or the standard error of the mean.
- It is OK to report 1-sigma error bars, but one should state it. The authors should preferably report a 2-sigma error bar than state that they have a 96% CI, if the hypothesis of Normality of errors is not verified.
- For asymmetric distributions, the authors should be careful not to show in tables or figures symmetric error bars that would yield results that are out of range (e.g. negative error rates).
- If error bars are reported in tables or plots, The authors should explain in the text how they were calculated and reference the corresponding figures or tables in the text.

8. **Experiments Compute Resources**

   Question: For each experiment, does the paper provide sufficient information on the computer resources (type of compute workers, memory, time of execution) needed to reproduce the experiments?

   Answer: [Yes]

   Justification: yes, details are provided in the implementation details section of results.

   Guidelines:

   - The answer NA means that the paper does not include experiments.
   - The paper should indicate the type of compute workers CPU or GPU, internal cluster, or cloud provider, including relevant memory and storage.
   - The paper should provide the amount of compute required for each of the individual experimental runs as well as estimate the total compute.
   - The paper should disclose whether the full research project required more compute than the experiments reported in the paper (e.g., preliminary or failed experiments that didn't make it into the paper).

9. **Code Of Ethics**

   Question: Does the research conducted in the paper conform, in every respect, with the NeurIPS Code of Ethics https://neurips.cc/public/EthicsGuidelines?

   Answer: [Yes]

   Justification: we follow the code of ethics.

   Guidelines:

   - The answer NA means that the authors have not reviewed the NeurIPS Code of Ethics.
   - If the authors answer No, they should explain the special circumstances that require a deviation from the Code of Ethics.
   - The authors should make sure to preserve anonymity (e.g., if there is a special consideration due to laws or regulations in their jurisdiction).

10. **Broader Impacts**

    Question: Does the paper discuss both potential positive societal impacts and negative societal impacts of the work performed?

    Answer: [NA]

    Justification: no societal impact of the work is apparent.

    Guidelines:

    - The answer NA means that there is no societal impact of the work performed.
    - If the authors answer NA or No, they should explain why their work has no societal impact or why the paper does not address societal impact.

https://doi.org/10.52202/079017-0050

- Examples of negative societal impacts include potential malicious or unintended uses (e.g., disinformation, generating fake profiles, surveillance), fairness considerations (e.g., deployment of technologies that could make decisions that unfairly impact specific groups), privacy considerations, and security considerations.
- The conference expects that many papers will be foundational research and not tied to particular applications, let alone deployments. However, if there is a direct path to any negative applications, the authors should point it out. For example, it is legitimate to point out that an improvement in the quality of generative models could be used to generate deepfakes for disinformation. On the other hand, it is not needed to point out that a generic algorithm for optimizing neural networks could enable people to train models that generate Deepfakes faster.
- The authors should consider possible harms that could arise when the technology is being used as intended and functioning correctly, harms that could arise when the technology is being used as intended but gives incorrect results, and harms following from (intentional or unintentional) misuse of the technology.
- If there are negative societal impacts, the authors could also discuss possible mitigation strategies (e.g., gated release of models, providing defenses in addition to attacks, mechanisms for monitoring misuse, mechanisms to monitor how a system learns from feedback over time, improving the efficiency and accessibility of ML).

11. **Safeguards**

    Question: Does the paper describe safeguards that have been put in place for responsible release of data or models that have a high risk for misuse (e.g., pretrained language models, image generators, or scraped datasets)?

    Answer: [NA]

    Justification: the paper poses no such risks.

    Guidelines:

    - The answer NA means that the paper poses no such risks.
    - Released models that have a high risk for misuse or dual-use should be released with necessary safeguards to allow for controlled use of the model, for example by requiring that users adhere to usage guidelines or restrictions to access the model or implementing safety filters.
    - Datasets that have been scraped from the Internet could pose safety risks. The authors should describe how they avoided releasing unsafe images.
    - We recognize that providing effective safeguards is challenging, and many papers do not require this, but we encourage authors to take this into account and make a best faith effort.

12. **Licenses for existing assets**

    Question: Are the creators or original owners of assets (e.g., code, data, models), used in the paper, properly credited and are the license and terms of use explicitly mentioned and properly respected?

    Answer: [Yes]

    Justification: we produced all codes and are original owner of assets. For third-party code, we explicitely cite and mark the dependency to those and credit the authors accordingly.

    Guidelines:

    - The answer NA means that the paper does not use existing assets.
    - The authors should cite the original paper that produced the code package or dataset.
    - The authors should state which version of the asset is used and, if possible, include a URL.
    - The name of the license (e.g., CC-BY 4.0) should be included for each asset.
    - For scraped data from a particular source (e.g., website), the copyright and terms of service of that source should be provided.

- If assets are released, the license, copyright information, and terms of use in the package should be provided. For popular datasets, `paperswithcode.com/datasets` has curated licenses for some datasets. Their licensing guide can help determine the license of a dataset.
- For existing datasets that are re-packaged, both the original license and the license of the derived asset (if it has changed) should be provided.
- If this information is not available online, the authors are encouraged to reach out to the asset's creators.

13. **New Assets**

    Question: Are new assets introduced in the paper well documented and is the documentation provided alongside the assets?

    Answer: [Yes]

    Justification: We provided detailed explanation in the paper, will have a documentation in the open-source code, and provide a detailed Supplementary Materials pdf with additional info.

    Guidelines:

    - The answer NA means that the paper does not release new assets.
    - Researchers should communicate the details of the dataset/code/model as part of their submissions via structured templates. This includes details about training, license, limitations, etc.
    - The paper should discuss whether and how consent was obtained from people whose asset is used.
    - At submission time, remember to anonymize your assets (if applicable). You can either create an anonymized URL or include an anonymized zip file.

14. **Crowdsourcing and Research with Human Subjects**

    Question: For crowdsourcing experiments and research with human subjects, does the paper include the full text of instructions given to participants and screenshots, if applicable, as well as details about compensation (if any)?

    Answer: [NA]

    Justification: the paper does not involve crowdsourcing nor research with human subjects.

    Guidelines:

    - The answer NA means that the paper does not involve crowdsourcing nor research with human subjects.
    - Including this information in the supplemental material is fine, but if the main contribution of the paper involves human subjects, then as much detail as possible should be included in the main paper.
    - According to the NeurIPS Code of Ethics, workers involved in data collection, curation, or other labor should be paid at least the minimum wage in the country of the data collector.

15. **Institutional Review Board (IRB) Approvals or Equivalent for Research with Human Subjects**

    Question: Does the paper describe potential risks incurred by study participants, whether such risks were disclosed to the subjects, and whether Institutional Review Board (IRB) approvals (or an equivalent approval/review based on the requirements of your country or institution) were obtained?

    Answer: [NA]

    Justification: the paper does not involve crowdsourcing nor research with human subjects.

    Guidelines:

    - The answer NA means that the paper does not involve crowdsourcing nor research with human subjects.

https://doi.org/10.52202/079017-0050

- Depending on the country in which research is conducted, IRB approval (or equivalent) may be required for any human subjects research. If you obtained IRB approval, you should clearly state this in the paper.
- We recognize that the procedures for this may vary significantly between institutions and locations, and we expect authors to adhere to the NeurIPS Code of Ethics and the guidelines for their institution.
- For initial submissions, do not include any information that would break anonymity (if applicable), such as the institution conducting the review.